The role of deformation-reaction interactions to localize strain in polymineralic rocks: Insights from experimentally deformed plagioclase-pyroxene assemblages

Nicolas Mansard, Holger Stünitz, Hugues Raimbourg, Jacques Précigout

To cite this version:

Nicolas Mansard, Holger Stünitz, Hugues Raimbourg, Jacques Précigout. The role of deformation-reaction interactions to localize strain in polymineralic rocks: Insights from experimentally deformed plagioclase-pyroxene assemblages. Journal of Structural Geology, 2020, 134, 104008 (18 p.). 10.1016/j.jsg.2020.104008 . insu-02476212

HAL Id: insu-02476212
https://insu.hal.science/insu-02476212v1

Submitted on 12 Feb 2020

The role of deformation-reaction interactions to localize strain in polymineralic rocks: Insights from experimentally deformed plagioclase-pyroxene assemblages

Nicolas Mansard, Holger Stünitz, Hugues Raimbourg, Jacques Précigout

PII: S0191-8141(19)30348-7

DOI: https://doi.org/10.1016/j.jsg.2020.104008

Reference: SG 104008

To appear in: *Journal of Structural Geology*

Received Date: 21 August 2019

Revised Date: 22 December 2019

Accepted Date: 2 February 2020

Please cite this article as: Mansard, N., Stünitz, H., Raimbourg, H., Précigout, J., The role of deformation-reaction interactions to localize strain in polymineralic rocks: Insights from experimentally deformed plagioclase-pyroxene assemblages, *Journal of Structural Geology* (2020), doi: https://doi.org/10.1016/j.jsg.2020.104008.

Author statement

Conflict of Interest

Potential conflict of interest exists:

We wish to draw the attention of the Editor to the following facts, which may be considered as potential conflicts of interest, and to significant financial contributions to this work:

The nature of potential conflict of interest is described below:

☒No conflict of interest exists.

We wish to confirm that there are no known conflicts of interest associated with this publication and there has been no significant financial support for this work that could have influenced its outcome.

Funding

☒Funding was received for this work.

All of the sources of funding for the work described in this publication are acknowledged below:

This work has received funding from the European Research Council (ERC) under the seventh Framework Programme of the European Union (ERC Advanced Grant, grant agreement No 290864, RHEOLITH), and from the Labex VOLTAIRE (ANR-10-LABX-100-01).

☐No funding was received for this work.

Intellectual Property

☒We confirm that we have given due consideration to the protection of intellectual property associated with this work and that there are no impediments to publication, including the timing of publication, with respect to intellectual property. In so doing we confirm that we have followed the regulations of our institutions concerning intellectual property.

We the undersigned agree with all of the above.

	Author's name (First, Last)	Signature	Date
1.	Nicolas Mansard		19/12/19
2.	Jacques PRÉCIGOUT		19/12/19
3.	Hugues RAINBOURG		19/12/19
4.	Holger Stunitz		20-12-2019

The role of deformation-reaction interactions to localize strain in polymineralic rocks: insights from experimentally deformed plagioclase-pyroxene assemblages

Nicolas Mansard[1,*], Holger Stünitz[1,2], Hugues Raimbourg[1] and Jacques Précigout[1]

[1] Institut des Sciences de la Terre d'Orléans (ISTO), UMR 7327, CNRS/BRGM, Université d'Orléans, 45071 Orléans, France
[2] Department of Geology, University of Tromsø, Dramsveien 201, 9037 Tromsø, Norway

To be published in Journal of Structural Geology.

*Corresponding author at : UMR 7327, Institut des Sciences de la Terre d'Orléans (ISTO), Université d'Orléans, 1A rue de la Férollerie, 45071 Orléans, France. Telephone numbers : +33 6 59 49 73 42.

E-mail adresses : *nicolas.mansard@cnrs-orleans.fr* *(N. Mansard),* *holger.stunitz@uit.no* *(H. Stünitz),* *hugues.raimbourg@univ-orleans.fr* *(H. Raimbourg),* *jacques.precigout@univ-orleans.fr* *(J. Précigout).*

Keywords: Rock deformation experiments; Mineral reactions; Diffusion creep; Strain localization.

Abstract

In order to study the mutual effect of deformation and mineral reactions, we have conducted shear experiments on fine-grained plagioclase-pyroxene assemblages in a Griggs-type solid-medium deformation apparatus. Experiments were performed at a constant shear strain rate of 10^{-5} s^{-1}, a confining pressure of 1 GPa and temperatures of 800, 850 and 900 °C. While the peak stress of plagioclase + orthopyroxene assemblages reaches values between those of the end-member phases, the strength of polymineralic materials strongly decreases after peak stress and reaches flow stresses that stabilize far below those of the weaker phase (plagioclase). This weakening correlates with the coeval development of high-strain shear zones where new phases are preferentially produced, including new pyroxene, plagioclase and amphibole. The reaction products mostly occur as intimately mixed phases within fine-grained and interconnected shear bands, together with different compositions with respect to the starting material. This indicates that deformation significantly enhances the kinetics of mineral reactions, which in turn strongly weaken the deforming sample, here attributed to a switch to grain-size-sensitive diffusion creep through phase nucleation and grain size reduction. Such an interplay between deformation and mineral reactions may have strong implications for the initiation, development, and durability of shear zones in the lower crust.

1. Introduction

Strain localization and resulting shear zones are considered to be fundamental features of plate tectonics on Earth (e.g. Tackley, 1998; Bercovici and Ricard, 2012). They accommodate a large amount of strain and have a direct control on rock rheology, so their development is critical to understanding the dynamics of the lithosphere. The formation of viscous shear zones has been considered to result from one or several processes of strain-induced weakening, which expresses as a stress drop at constant strain rate or an increase of strain rate at constant stress (e.g. Paterson, 2013). Possible weakening mechanisms include: (1) Geometric and/or fabric softening, (2) a change in deformation mechanism, commonly due to grain size reduction, (3) fracturing, (4) metamorphic mineral reactions, (5) shear heating (6) water- or (7) melt-induced weakening (e.g. Poirier, 1980; White et al. 1980; Burlini and Bruhn, 2005). While some of these mechanisms apply to monophase rocks, others are more typical of polyphase materials.

As a starting point, laboratory-derived flow laws have been determined for the deformation of monophase materials to understand the rheology of important rock-forming minerals in the viscous regime of the lithosphere, including olivine (e.g., Chopra and Paterson, 1981), quartz (Paterson and Luan, 1990), plagioclase (Rybacki and Dresen, 2000; Dimanov et al., 1999) and pyroxene (Bystricky and Mackwell, 2001). For instance, the experiments of, e.g., Rybacki and Dresen, (2000) and Chen et al., (2006), have shown that water may considerably reduce the strength of feldspar and pyroxene aggregates. Plastic flow and grain size reduction by dynamic recrystallization are also best described in deformation experiments of monophase materials, giving rise to state-of-the-art flow laws (e.g. White et al. 1980, Schmid 1982, Rutter and Brodie, 1988). These experiments highlighted a potential source of weakening induced by a transition from grain-size-insensitive to grain-size sensitive creep, but this transition is not expected to cause long-term weakening in monophase aggregates, because the efficient grain growth at elevated temperature is expected to counteract the weakening effect of grain size reduction (e.g. Rutter and Brodie, 1988, De Bresser et al., 2001).

Except for rare cases, the lithosphere consists of polyphase rocks. Thus, a growing body of literature has also addressed the rheology of polyphase material, given the fact that such a rheology is likely to be different from that of monophase ones (e.g. Bürgmann and Dresen, 2008). For instance, the presence of additional phases in polyphase aggregates inhibits grain growth and controls microstructures through pinning (e.g. Olgaard and Evans, 1986; Herwegh et al., 2011). The dominant deformation mechanism can thus be expected to differ as a consequence of phase interactions.

In this context, the rheology of polyphase aggregates for gabbroic composition has a fundamental importance for understanding the mechanical behaviour of the oceanic and lower crusts; mafics are the most abundant rock types in these crustal layers (e.g. Weaver and Tarney, 1984; Christensen and Mooney, 1995). However, experimental studies of high-temperature deformation of gabbroic composition are still comparatively rare (e.g. Dimanov et al., 2003, 2007; Dimanov and Dresen, 2005), and these studies have not considered mineral reactions. They focused indeed on the role of secondary phases, grain size, water content, stress and spatial distribution of grains to account for changing flow stress and dominant deformation mechanism in polyphase feldspar-pyroxene aggregates. Yet, other studies suggest that the occurrence of mineral reactions during viscous flow may have the potential to weaken rocks and consequently localize strain (e.g. Stünitz and Tullis, 2001; De Ronde et al., 2004, 2005; Getsinger and Hirth, 2014; Marti et al., 2017, 2018).

Strain localization and weakening in viscous shear zones as a result of mineral reactions are mostly achieved through changes in P-T conditions (e.g. Gapais, 1989; Newman et al., 1999) or through fluid-rock interactions (e.g. Austrheim, 1987; Menegon et al., 2015). Changes in P-T conditions commonly occur during oceanic and continental subduction and exhumation along crustal-scale shear zones, where the thermodynamic disequilibrium promotes the growth of new stable minerals (e.g. Gerya et al., 2002; Jamtveit et al., 2016). In addition, shear zones represent permeable pathways for fluids that enhance diffusion and strongly catalyse mineral reactions under both, low (e.g. Fitz Gerald and Stünitz, 1993; Newman and Mitra, 1993; Mansard et al., 2018) and high metamorphic grades (e.g. Brodie, 1980; Boundy et al., 1992; Glodny et al., 2003). The importance of mineral reactions lies in the possible grain size reduction and change in deformation mechanism leading to a switch from grain-size-insensitive to grain-size sensitive creep, giving rise to substantial weakening (e.g. Etheridge and Wilkie, 1979; Olgaard, 1990; Stünitz and Fitz Gerald, 1993; Fliervoet et al., 1997; De Bresser et al., 1998; Kruse and Stünitz, 1999; De Bresser et al., 2001; Kenkmann and Dresen, 2002; Precigout et al., 2007; Raimbourg et al., 2008; Linckens et al., 2011; Kilian et al., 2011; Viegas et al., 2016). Mineral reactions also contribute to form mixing zones that play an important role of weakening because the pinning of grain boundaries impedes grain growth and keep the grain size small (e.g. Etheridge and Wilkie, 1979; Herwegh et al., 2011).

In this contribution, rock deformation experiments on H_2O-added plagioclase-orthopyroxene samples were performed to investigate the rheology and evolution of microstructures with increasing strain. The experiments provide insight into weakening mechanisms and localization of deformation during shear zone development. This study presents a simplified model example of how deformation can facilitate metamorphic reactions, heterogeneous nucleation, formation of fine-grained phase mixtures, and how conversely such an evolution in microstructures eventually results in strain localization and weakening of polyphase aggregates. The study also demonstrates the importance of interaction of individual phases in polymineralic assemblages when dealing with the behaviour of the lithosphere.

2. Methods

2.1 Experimental procedure

The shear deformation experiments were carried out in two Tullis-modified Griggs-type deformation apparatus at the University of Tromsø (Norway) and in a new generation Griggs rig at the University of Orléans (France). The following sections briefly describe the preparation of the sample assembly and experimental procedure.

2.1.1 Starting material and sample preparation

Experiments were performed on two-phase plagioclase-orthopyroxene assemblages and, for comparison, pure plagioclase and pure orthopyroxene (Opx) material. The starting material was prepared from gem-quality Sonora labradorite (An_{60}), and Damaping opx from peridotite (Opx: Wo_1-En_{89}-Fs_{10}). The initial mineral compositions are presented in Table 1. The rocks were crushed using a hammer and sieved to sizes grains diameter between 100 to 200 µm. Minerals were pre-separated with a Frantz magnetic separator and hand-picked. They were subsequently crushed into an alumina mortar, and then a powder ranging from 10 to 20 µm grain size was extracted by settling in a distilled water column. Opx and plagioclase powders were mixed at a ratio of 50 : 50% (by volume) as a slurry in acetone using an ultrasonic stirrer to avoid density/grain size separation (De Ronde et al., 2004, 2005). (*insert Table 1*).

The mixed powder was placed between 45° pre-cut alumina forcing blocks (Fig. 1). An amount of ~0.12 g powder for 6.33 mm diameter samples (at Tromsø University) or 0.25 g for 8 mm diameter samples (at Orléans University) were used with 0.1 wt. % H_2O added to all samples, resulting in a shear zone of ~1 mm thickness. A nickel foil of 0.025 mm thickness was wrapped around the pistons and all inserted into a weld-sealed platinum jacket. NaCl was used as solid confining medium and the temperature was controlled by a S-type (Pt/Pt-Rh) thermocouple. Detailed descriptions of the sample assembly in the Griggs-type deformation apparatus are given in Pec et al., 2012, Marti et al., 2017 and Précigout et al., 2018. (*insert Fig. 1*).

2.1.2 Deformation experiments

Samples were deformed at constant shear strain rate of ~10^{-5} s^{-1} to varying amounts of shear strain (see Table 2 for a summary of experimental conditions). Pressures and temperatures were increased alternatingly over several hours to achieve the target values of 800, 850, and 900°C and confining pressures of 1.0 GPa (Précigout et al., 2018). At the desired P-T conditions, a period of hydrostatic hot-pressing was applied. The deformation part of the experiment was started by advancing the deformation piston first through the lead piece and then touching the upper forcing block (hit point), indicating the starting point of sample deformation. The displacement of the deformation piston within the lead piece is characterized by a slow increase of differential stress (‘run-in’ curve; Précigout et al., 2018), the duration of which may vary depending on the experiment. We thus separated the experiments with a relatively short (< 70h) and long (> 70h) “run-in” period. Following this period, samples were deformed to shear strains of up to $\gamma = 8$ (high shear strain experiments). Several experiments were also carried out without deformation (hot-pressing experiments) or with deformation only up to the peak stress at $\gamma \approx 1$ (peak stress experiments) in order to study the early stages of deformation. The longer run-in periods cause reaction products to nucleate before deformation starts, whereas shorter run-in periods cause reaction products to form only during deformation, allowing to study the relationship between the amount of reaction products over time and the effect of deformation. Experiments reaching similar shear strain with different total durations can be compared (*insert Table 2*).

When deformation was stopped, samples were quenched to 200°C within minutes (temperature drop of ~150 to 300 °C/min) to preserve the deformation microstructures. Subsequently, the force and confining pressure were decreased simultaneously to room pressure and room temperature conditions. During initial stages of the decompression, the differential stress is kept above the confining pressure (~ 100 to 200 MPa) to prevent the formation of unloading cracks. After the experiment, the samples were impregnated with epoxy resin and sectioned along the piston axis and parallel to the shear direction to produce thin sections.

Experimental data were digitally recorded using the Catman Easy data acquisition system and processed using a MATLAB-based program inspired from the "rig" program of Matej Pec (Pec et al., 2016) and available at https://sites.google.com/site/jacquesprecigout/telechargements-downloads. The hit point was defined by curve fitting and the stress-strain curves of the deformed samples were then generated by applying corrections on the displacement and force curves considering the rig stiffness and friction of the apparatus, respectively. Furthermore, the sample compaction and surface change (pistons overlap) were corrected to the displacement over the whole period of sample deformation. The stress correction of Holyoke and Kronenberg (2010) was not applied.

2.2 Analytical procedure

After the experiment, samples were cut along the piston axis in the plane of maximum displacement and vacuum-impregnated with low viscosity epoxy to prepare thin sections for microstructural analysis. The samples were mainly analysed using light and scanning electron microscopy (SEM – TESCAN MIRA 3 XMU) at the ISTO-BRGM (Orléans, France). Starting mineral compositions were determined using electron microprobe CAMECA SX Five (EPMA) at the ISTO-BRGM (Orléans, France) on carbon-coated (20 nm thickness) thin sections at 12 or 15 kV and a beam size of ca. 1 µm. We have analysed the core and rim composition of plagioclase and pyroxene grains in deformed assemblages by EDS. In the mixed zones, the plagioclase-pyroxene compositions were also analysed if the grain size was sufficiently large. The amphibole composition is based on composition of large grains in low-strain zones, because in high-strain zones, individual grains are typically too small to be analysed. Representative analyses of these chemical compositions are given in Table 3. (*insert Table 3*)

2.3 Microstructural analysis

Different mineral grains were identified in backscatter electron (BSE) images. Grain shape preferred orientations (SPO) were analysed from manually produced bitmap images using the autocorrelation function (ACF; Panozzo, 1983; Heilbronner, 2002). The ACF was calculated for both, all combined phases (bulk ACF) and each individual phase (local ACF). Because individual grain boundaries are difficult to distinguish (different from phase boundaries which are obvious in BSE images), the ACF is used because it does not require segmentation of the individual grains. This method thus avoids errors and biases caused by the identification of individual grains. For further details about equations related to the ACF, the reader is invited to consult the original study of Heilbronner (1992).

Scanning electron microscope/backscattered electron (SEM/BSE) images were used to produce manually digitized phase maps, which allowed the analysis of grain size. The grain size was defined as the equivalent circular area diameter ($d_{equ} = 2 \times \sqrt{\frac{area}{\pi}}$) (Heilbronner and Barrett, 2014), and measured using the public domain software ImageJ (http://rsb.info.nih.gov/ij/).

3. Results

3.1. Mechanical data

The terminology used to describe stress-strain curves is explained in Fig. 2a. While the same colour code is used for different temperatures, a cross on the stress-strain-curve indicates when the forcing blocks started to slip at the sample interface.

3.1.1 Pure plagioclase and pyroxene samples

The pure plagioclase experiments at 800 °C and 900 °C show similar types of stress-strain curves. At 800 °C the sample shows more than 200 MPa higher flow stress than the sample deformed at 900 °C (Fig. 2b), and both samples deform at stresses below the Goetze criterion. The Goetze criterion ($\Delta\sigma \leq P_{conf}$) is used as an empirical criterion to delineate stress conditions where rocks deform plastically (Kohlstedt et al., 1995). In both experiments, the differential stress slightly decreases after reaching a peak stress at $\gamma < 1$ (Fig. 2b). The pure pyroxene experiment was performed on a larger initial grain size fraction (powder sieved to extract a grain fraction ≤ 40 µm) than that of the other experiments (10 to 20 µm). The pure orthopyroxene is very strong at 900 °C, reaching a peak stress of ~1600 MPa at γ ~0.6, well above the Goetze criterion (Fig. 2b). The experiment was stopped during the stress drop as only brittle deformation was expected to occur at these high differential stresses.

3.1.2 Plagioclase -orthopyroxene mixtures

The experiments on phase mixtures can be divided into two different series depending on the time spent at P-T conditions before the contact between the σ_1 piston and top alumina piston (hit point). After a short "run-in" period (< 70h at temperature and pressure conditions before hit point), the orthopyroxene + plagioclase (Opx + Plag) mixtures are very strong at 800 °C (559NM) and 850 °C (557NM), reaching a peak stress of ~ 1100 MPa at γ ~ 0.3 (Fig. 2c). Slip at one of the sample/forcing block interfaces causes Δσ to drop far below the Goetze criterion. The samples deformed at 900°C show peak stress values close to those at 800 and 850 °C, but at higher shear strain (γ ~1.5). At 900 °C, there is a gradual and pronounced weakening after peak stress. In one case, slip occurred at the forcing block interface (Fig. 2c), and the differential stress decreases below the Goetze criterion before stabilizing around 800 MPa (OR49NM). In the other case, the sample weakens continuously with a reduction of ~50% in differential stress (Fig. 2c), until reaching a quasi-steady-state shear stress around 550 MPa near γ ~ 6.5 (OR41NM). (*insert Fig. 2*).

After a longer "run-in" period at 800 °C (Fig. 2d; > 70h at temperature and pressure conditions before the hit point), a stress drop occurs at a peak stress value near γ ~0.7 (above the Goetze criterion at ∼1250 MPa; Fig. 2d), probably caused by slip at one sample-forcing block interface (OR24NM). In contrast, the other samples at 850 °C (OR38NM) and 900 °C (OR34NM) weaken continuously after peak stress, and then approach a quasi-steady-state shear stress at γ ~7.8 and γ ~6, respectively (Fig. 2d). In these last two experiments, the weakening is very pronounced with ~64 % of weakening for the 850 °C sample and ~78 % for the 900 °C sample compared to peak stress values. The Opx + Plag mixtures show a slightly less steep loading curve compared to shorter run-in period experiments (Fig. 2d), indicating a lower strength of the samples (the loading curve in the solid-medium apparatus at high temperatures is not a purely elastic, but involves a component of permanent sample strain; Richter et al. 2018).

These sets of experiments (Fig. 2) demonstrate that pure phase samples are either very strong and deform only in the brittle field (Opx), or relatively weak and deform plastically (Plag) at a moderate to low flow stress without significant weakening after peak stress. The initial strength of mixed phase samples (peak stress) lies between the two extreme values of the pure phase samples, but the mixed phase samples weaken after peak stress and give rise to a final strength far weaker than the weakest of our mono-phase samples (i.e., pure plagioclase).

3.2 Microfabrics and composition

3.2.1 Pure end-member experiments

The pure Plag samples deformed at 800 °C and 900 °C are microstructurally similar to one another and show homogeneous deformation. Although it is difficult to distinguish all individual plagioclase grains in BSE images, there is a clear plagioclase grain size refinement locally (Fig. 3a). Recrystallized grains do not show different chemical composition with respect to the relict grains. While our experiments are stronger than those carried out by Stünitz and Tullis (2001) (~550 MPa compared to ~360 MPa, but the grain size ranges between 6 and 10 μm in Stünitz and Tullis (2001); it was between 10 and 20μm in this study), the microstructures are similar and no reaction products are formed at the P-T conditions imposed.

The pure Opx sample with larger initial grain size (≤ 40 μm compared to 10-20 μm of all other samples) deformed at 900 °C shows extensive fracturing, indicative of brittle deformation (Fig. 3b). The pervasive fractures result in a locally dramatically reduced pyroxene grain size (down to < 1 μm; Fig. 3c). No indication for plastic deformation was detected. (*insert Fig. 3*).

3.2.2 Mixed phase samples

3.2.2.1 High shear strain samples

3.2.2.1.1 General features

At 850 °C, the high-strain sample is characterized by a single high-strain zone that traverses the sample through the centre from one interface of the forcing block to the other (Fig. 4). The reaction products appear pervasively in the whole sample, but the high-strain zone contains considerably more reaction products (~80%) than the low-strain one (~28%) (determined from BSE images). The grain size of the reaction products is substantially reduced in the high-strain zone with respect to the low-strain regions, where the reaction products develop as coronas at the Opx_1-$Plag_1$ boundaries or as monophase aggregates without the development of mixed phase zones (Fig. 5a). The reaction products are identified as newly-formed pyroxene (Opx_2), plagioclase ($Plag_2$) and amphibole (Amph); all of which were absent from the starting material. The original Opx_1 clasts are locally cut by brittle fractures, reducing the grain size slightly (Fig. 5b), and the fractures are filled with Opx_2 reaction products. The transition between low- and high-strain zones can locally be gradual and shows the incipient mixing of phases at the edges of original Opx_1 (Fig. 5c-d). The reaction progressively consumes the pre-existing Opx_1 and induces the development of σ-tails parallel to the shear direction. These tails locally coalesce and form interconnected shear bands of fine-grained reaction products composed of Opx_2, $Plag_2$ and locally subordinate Amph, which usually have rounded grain shapes (Fig. 5c-d). (*insert Fig. 4*).

3.2.2.1.2 High-strain zones

Reactions in high-strain zones result in intense grain size reduction and in coalescence of foliation-forming aggregates of fine grains into mixed phase shear bands, usually laterally connected (Fig. 5e-f, 6). Some of the shear bands have a synthetic orientation with respect to the bulk shear zone (C´-type orientation in the sense of Berthé et al., 1979), many of them are parallel to the shear direction (C-type orientation). At 850 °C, the majority of shear bands are organized within high-strain zones of ~250-300 µm thick (Fig. 6a-b). Similar features are shared at 900 °C, although deformation is more distributed (Fig. 6c-d-e). (*insert Fig. 5*).

The modal proportion of the reaction products reaches locally 80% in the high-strain zones, as these products replace most of the pre-existing large grains, including the original $Plag_1$ (Fig. 7a). Thus, most of the fine-grained mixed phase shear bands are composed of reaction products (Opx_2, $Plag_2$ and Amph with minor amount of quartz (Qtz)). The high-strain zones still comprise some original Opx_1 clasts that are embedded in the fine-grained reaction products (Fig. 5e), but these clasts are reduced in size (from reaction) and appear less elongated compared to those of the low-strain zones (Fig. 7b). The Opx_1 appears therefore as a mechanically rigid clast within weaker mixed zones of reaction products, the grain size of which is typically below one micron. (*insert Fig. 6*).

The strain is semi-quantitatively estimated from the aspect ratio of the bulk fabric determined by the ACF and angle of the long axis of the bulk ACF with respect to the shear plane (Fig. 7). It should be noted that this method of strain estimate is not an exact strain analysis, given the absence of passive markers or rigid particles with a known orientation before deformation (see also discussion in De Ronde et al. 2004). There is a gradient in the aspect ratio and the orientation of reaction products between low- and high-strain zones. The bulk aspect ratio is higher in the high-strain zones, where the amount of reaction products is the most abundant (Fig. 7). Moreover, the bulk aspect ratio is around one and a half times higher in the high-strain zones compared to the low-strain ones. The reaction products in the high strain zones are strongly oriented subparallel to the shear plane (piston interface) (Fig. 7d; α between ~ 3° and 5°). In the low strain zones, the angle between the long axis of the fabric of reaction products and the shear plane is higher (Fig. 7d; $\alpha \sim 9°$). By applying the equation that relates the preferred orientation of passive lines with respect to the shear plane ($\gamma = 2/\tan 2\theta$; Ramsay, 1980), we can estimate that local shear strain reaches γ ~11 to 16 in the high-strain zones and $\gamma \sim 6$ in the low-strain ones. (*insert Fig. 7*).

3.2.1.2.3 Mineral chemistry

Overall, major compositional changes in plagioclase and opx occur together with grain size reduction in the shear zones (Fig. 8a-b). The chemical composition of new grains of plagioclase and opx distinctly differs from that of relict clasts. While the chemical composition of clasts is mostly An59, the new reaction rim ($Plag_2$) is more albitic (An52; Fig. 8a). The reaction also results in almost complete disappearance of $Plag_1$ in the high-strain zones (Fig. 7a), and within mixed phase zones and shear bands, the anorthite component of fine-grained $Plag_2$ is slightly lower than that of new rims (An49).

The chemical composition of clasts (Opx_1) varies from En(86) to En(90), while the rim composition (Opx_2) shows a decreasing enstatite content down to En(82) (Fig. 8b). The composition of fine-grained new Opx_2 in the high-strain zone decreases even more to En(79). The reaction products are thus characterized by an enrichment in iron content, together with the formation of new amphibole grains enriched in Mg and depleted in Fe. New amphibole grains appears in both, more and less deformed zones, but they are more abundant in fine-grained shear bands and in the sample deformed at 850 °C (OR38NM – strain is highly localized in this sample). Based on the composition of larger reaction products in the low-strain zones – the grain size is too small in shear bands of the high-strain zones to measure the composition of individual grains – amphiboles are classified as magnesio-hornblende and tschermakite (Fig. 8c). (*insert Fig. 8*).

3.2.2 Hot-pressing and peak stress experiments

For comparisons with deformed samples, some samples have been hot-pressed (without deformation) as long as the experiment duration of the high shear strain samples. At 900 °C, hot-pressing samples of Opx + Plag show the development of reaction products (Fig. 9a-b) with the same composition of Opx_2, $Plag_2$ and Amph as the deformed samples. The reaction products occur as thin coronas at the Opx_1-$Plag_1$ phase boundaries or in cracks. The volume of reaction products reaches about 3% in the sample held for 100h and about 10% in the one held at the same pressure and temperature for 193h. The rims grow concentrically around old grain relicts in hot-pressed samples and therefore do not nucleate in specific locations at plagioclase-pyroxene phase boundaries (Fig. 9a). However, in the sample held at pressure and temperature for 193h, the rims are slightly thicker and locally some aggregates of original Opx_1 are replaced by Opx_2 (Fig. 9c).

In samples where the deformation was stopped at peak stress (OR47NM and OR51NM), the microstructures differ slightly in the amount of reaction products and their arrangement with respect to the microstructures of the hot-pressing experiments (Fig. 9d-e). Indeed, the amount of reaction products slightly increase in peak stress experiments compared to the hot-pressing ones. The reaction products are relatively homogeneously distributed in the samples, although they start to coalesce locally to form partially connected aggregates (Fig. 9e). The original Opx_1 and $Plag_1$ grains are also slightly elongated in the flow direction. When these experiments reach relatively high conditions of differential stress, close to the Goetze criterion, fractures locally affect the pyroxene and cause a slight reduction in grain size. (*insert Fig. 9*).

3.2.3 Intermediate shear strain experiment

One sample was taken to a lower strain and is considered as a sample of intermediate strain between peak stress and high shear strain (Fig. 2c; OR49NM; the distance between the cross and the second cusp in the curve represents slip on the interface and thus a sample strain of $\gamma \sim 5$ is achieved). This sample is characterized by the development of subparallel fine-grained polyphase shear bands (Fig. 10a), both composed of an intimate mixture of fine-grained Opx_2, $Plag_2$ and Amph (grain size << 1 μm; Fig. 10b). The shear bands originate from tails that extend from the edges of original Opx_1 (Fig. 10c), and progressively coalesce to form an interconnected network (Fig. 10a). (*insert Fig. 10*).

3.3 Grain size

The overall grain size for both plagioclase and opx grains is strongly reduced with increasing strain. Most of the opx grain size reduction occurs after the peak stress, and hence, during the weakening and development of fine-grained mixed phase zones (Fig. 11). While the original opx grain size remains almost unchanged at peak stress with respect to the starting material (cracking refines the grain size to a mode of 15.6 µm), the size of opx grains in the reaction products strongly decreases in mixed phase zones at high shear strain (mode of distribution = 0.2 µm). To ensure accurate grain size determination, we have excluded plagioclase from the measurements because of the difficulty to distinguish individual grains in plagioclase aggregates. Despite this issue, visual inspection suggests that the plagioclase grain size in stable fine-grained mixtures is similar to that of opx. (*insert Fig. 11*).

3.4 Reaction progress

The set of experiments performed at different durations and 900 °C is used to illustrate the relation between the volume fraction of reaction products with time and the effect of deformation on reaction (Fig. 12). The volume fraction of reaction products increases from ~3% for 100h to ~10% at 193h if deformation is not applied (OR55NM and OR43NM) (Fig. 12a). In contrast, even after a short period of deformation to small strain at peak stress, the volume fraction of reaction products increases to ~11% (OR47NM) and ~18% (OR51NM) (Fig. 12a). This amount of reaction products is higher than the amount documented for the hot-pressing experiment with equivalent duration. With increasing strain, the amount of reaction products also increases and reaches 26% (OR49NM), 35% (OR41NM) and 43% (OR34NM) (Fig. 12a). (*insert Fig. 12*).

4. Discussion

4.1 Mechanical data – strength of single- and two-phased assemblages

The mechanical data of our experiments show a systematic difference in the rheological evolution between monomineralic samples (Opx or Plag) and phase mixtures (Fig. 2). The monomineralic samples either deform by brittle mechanisms only (Opx; the experiment was stopped before failing completely), or they deform viscously at steady state stresses following a weakening of less than 150 MPa (Plag). The deformation of pure Opx also gives rise to high differential stress at 900 °C ($\Delta\sigma$ ~1600 MPa; Fig. 2b). Advances in rock deformation studies provided detailed documentation about the creep behaviour of pyroxene (e.g. Bystricky and Mackwell, 2001; Dimanov et al., 2003, 2005; Chen et al., 2006), but mostly for Cpx; the mechanical data for Opx is indeed limited and restricted to dry Opx only (Bruijn and Skemer, 2014; Bystricky et al., 2016). Nevertheless, based on deformation mechanism maps (Fig. 13), our deformation conditions involve a far higher strain rate – of several orders of magnitude – than the one predicted by the dislocation creep flow law of Bystricky et al. (2016). Even the weaker wet Cpx flow law of Dimanov and Dresen (2005) still indicates strain rates that are one order of magnitude lower than our applied strain rates (Fig. 13b). Thus, dislocation creep deformation of Opx is not expected to accommodate the applied strain rates in our samples, in agreement with the observed brittle behaviour of the pure Opx sample (Fig. 3b). For pure Plag, our flow stresses at the given strain rate for $\gamma > 2$ (= steady state conditions) are in good agreement (Fig. 13c) with the flow law from Rybacki and Dresen (2000) using the conversion between simple shear and coaxial strain rates of $\dot{\varepsilon} = \dot{\gamma} / \sqrt{3}$ (Gerya, 2010; Tokle et al., 2019). Our results for pure phase Plag and Opx are thus consistent with previous results found in the literature. (*insert Fig. 13*).

The mixed Opx + Plag samples deform under continuous weakening after attaining a peak stress, the value of which is intermediate between the end-member strengths of Opx and Plag, in agreement with a Reuss-Voigt- or Taylor-Sachs model of phase mixture (e.g., Dimanov and Dresen, 2005). However, the Opx in our case is stronger than Cpx and deforms only by brittle processes, so that the peak strength of the 2-phase composite sample is between the two end-members and near the Goetze criterion (Fig. 2). In addition, the pronounced weakening after peak stress produces final flow stresses up to 800 MPa that are far below the Goetze criterion ($\Delta\sigma \leq P_{conf}$), and below the end-member strength of the weaker phase, i.e., plag. This suggests that the deformation mechanism of the phase mixture differs from those of the end-members, because the strength of the composite should lie between the end-member strengths of a Reuss-Voigt or Taylor-Sachs-model. As discussed below, such a different rheological evolution may be explained by the progressive modification of the phase assemblage and microstructure through chemical interactions, i.e., mineral reactions.

4.2. Nucleation and grain size reduction

From figures 4 to 7, the local zones of reaction products accommodate far more strain than the relict phases Opx and Plag, so that the reaction products are responsible for the mechanical weakening of the samples. In addition, the microstructures at peak stress conditions mainly consist of coronas with only very little mixed phase material (Fig. 9d-e). Hence, most of the phase mixing starts after peak stress. Reaction products have a very small grain size of ~0.2 μm (Fig. 11). As the intense grain size reduction and phase mixing both start to appear after peak stress (Fig. 14), strain weakening and strain partitioning into the high-strain zones (Fig. 6) likely commence as a consequence of these two processes.

There is no flow law for Plag + Opx mixtures, and composite flow laws only exist for Cpx + Plag (Dimanov and Dresen, 2005). We thus plotted the grain size modes and means of the fine-grained reaction products (Opx + Plag) against the bulk stresses of the related experiment into the existing dry Opx, wet Cpx and wet Plag deformation mechanisms maps for a semi-quantitative comparison. The grain sizes and stresses of Opx_2 in the high-strain zones plot in the diffusion creep field (Fig. 13a-b). According to the Bruijn and Skemer (2014) data, pure Opx would still deform at one order of magnitude lower strain rates than our applied strain rates ($\sim 10^{-5}$ s^{-1}) in the diffusion creep regime (Fig. 13a). The Plag at the same grain size and stresses plots at an order of magnitude higher strain rates than those applied in our experiments (Fig. 13c). Because of strain partitioning, the expected strain rates in the high-strain zones are higher than the bulk ones by a factor of 2 to 3. From the semi-quantitative estimate of the deformation mechanism maps, the observed strain rates in the diffusion creep field for the fine grained Plag - Opx phase mixtures are compatible with those of the existing Cpx data and even slower than those for Plag from existing experimental data (Fig. 13). Thus, accommodation of deformation by diffusion creep in fine grained reaction products is roughly consistent with available rheological data for pyroxene and plagioclase for this deformation mechanism.

Several processes are generally invoked to account for phase transformations that may reduce grain size and promote phase mixing, influencing the rock strength. Some workers proposed that melt reactions may strongly influence the mechanical behaviour of rocks of the lower crust by inducing phase mixing and introducing a low viscosity melt in the system (e.g. Rosenberg and Handy, 2005). In our case, the P-T conditions are definitely outside of the melt-forming field, in agreement with the lack of melt in our samples. Another weakening process may involve dynamic recrystallization in the regime 1 of Hirth and Tullis (1992), i.e., where dynamic recrystallization mostly occurs by bulging. However, dynamic recrystallization does not produce phase mixing, and the pyroxene grain size in zones of mixed phase reaction products falls far below the orthopyroxene piezometer (Fig. 13; Linckens et al., 2014). Furthermore, the new Opx_2-grains have a different chemical composition compared to the starting material (Fig. 8), which excludes fracturing as a source of extensive grain size comminution (e.g. Ree et al., 2005; Park et al., 2006; Pec et al., 2012, 2016). In low-strain zones of samples that reach high differential stress conditions, discrete fractures segment Opx_1 clasts, but the fragments have a much larger grain size than the fine grains in high-strain zones. In contrast, phase nucleation as comminution process and a switch to grain size sensitive diffusion creep has been described in previous studies (e.g. Kilian et al., 2011; Herwegh et al., 2011; Wassmann and Stoeckhert, 2013; Hidas et al., 2016; Précigout and Stünitz, 2016; Marti et al., 2018; Prigent et al., 2018). Such a phase nucleation accounts for changing chemistry, phase mixing, and extensive grain size reduction in our experiments. (*insert Fig. 14*).

4.3 Mineral reaction and diffusion creep

While the development of reaction coronas induces limited grain size reduction and no phase mixing in low-strain zones (Fig. 5a-b, 14), the grain size reduction is much more intense in high-strain zones, combined with phase mixing (Fig. 5e-f, 6, 14). At the margin of high-strain zones, the early stages of phase mixing are preserved (Fig. 5c-d, 14). Fine-grained shear bands composed of Opx_2, $Plag_2$ and subordinate Amph extend at the edges of Opx_1 clasts and progressively replace the original $Plag_1$ (Fig. 5c-d). The phase mixing starts at the edges of the original Opx_1 that is gradually consumed by the reaction as evidenced by irregular Opx_1 boundaries, where new grains nucleate along low-stress sites (Fig. 5c). These microstructures suggest that diffusive mass transport takes place as part of the reaction. Nucleation of new grains of strongly reduced size facilitate diffusion creep. Phase mixing may stabilize the grain size by impeding grain growth. Previous studies also showed that phase nucleation forming tails at the expense of clasts may increase the degree of mixing in natural shear zones and experimental samples (e.g. Kruse and Stünitz, 1999; De Ronde et al., 2004; 2005; Holyoke and Tullis, 2006a, 2006b, Kilian et al., 2011, Tasaka et al. 2017, Mansard et al., 2018).

In our experiments, no grain growth is observed in fine-grained shear zones, even for longer experiments. This indicates that the occurrence of phase mixing has probably caused pinning of grain boundaries, impeding grain growth and preserving a fine grain size (e.g. Fliervoet et al., 1997; Herwegh et al., 2011; Kilian et al., 2011, Platt, 2015; Tasaka et al. 2017). Together with our predictions based on deformation maps, these features suggest that high-strain shear bands mostly deformed by diffusion creep. One important accommodation process to consider in this regime is grain boundary sliding (GBS; e.g, Langdon, 2006). In a reacting and simultaneously deforming mineral assemblage, GBS has a two-fold effect: (a) it creates new contact surfaces for reaction and (b) it produces potential cavitation sites, where new phases can nucleate (e.g., Kilian et al., 2011, Menegon et al., 2015, Précigout and Stünitz, 2016; Précigout et al., 2017; 2019). In this way, phase mixing is promoted in agreement with 1) the nucleation of fine grains (Fig. 11), 2) an intimate mixing of phases in high-strain zones (Fig. 5e-f, 6), and 3) the fact that the grain size of pyroxene and plagioclase falls within the diffusion creep field (Fig. 13). A switch of deformation mechanism to diffusion creep accounts here for a significant weakening and related strain localization into fine-grained high-strain zones, which hence constitute the weakest parts of the sample (e.g. Schmid et al., 1980, Rutter and Brodie, 1988; Montési, 2007; Precigout et al., 2007; Raimbourg et al., 2008; Gueydan et al., 2014).

4.4 Geometrical aspects: connectivity of shear zones and weakening processes

Previous works have shown that the rheological behaviour of rocks and strain localization can be highly dependent on strength contrast between phases, spatial geometry and amount of mineral reactions (e.g., Handy, 1990; Dell'Angelo and Tullis, 1996; Holyoke and Tullis, 2006a; Hansen et al., 2012). Holyoke and Tullis (2006a) found in high-temperature experiments a strong relation between the interconnection of weaker phases and strain localization. It has also been shown by Pec et al., (2016) and Palazzin et al., (2018) that the bulk strength of a given sample remains high if the weak shear bands are not, or poorly connected. Numerical studies also support the idea that phase arrangement can dramatically affect the bulk strength (e.g. Montési, 2007, Montési, 2013; Gerbi et al., 2016). In our study, the fine-grained shear bands are highly connected and oriented sub-parallel to the shear plane, suggesting that the reaction products connect in three dimensions and therefore control the bulk strength of the sample. This arrangement is considered as a type of geometric weakening (e.g. Handy, 1994; Dell'Angelo and Tullis, 1996; Holyoke and Tullis, 2006a; Gerbi et al., 2016). In addition, reaction progress will introduce more of the weak fine-grained material, increasing the probability of reaction products to connect after peak stress, and hence to promote further weakening. Previous shear deformation studies also described the formation of shear bands after peak stress (e.g. Holyoke and Tullis, 2006a; Pec et al., 2016; Marti et al., 2018). However, unlike our study, they do not always show the coalescence of shear bands into a connected high-strain zone that runs throughout the shear zone in high shear strain experiments (Fig. 4).

To summarize, our results support the idea that the sample weakening is dependent on two processes: (1) the introduction of fine-grained reaction products, and (2) their connectivity, which increases with an increasing amount of reaction products. The connectivity is nevertheless a complex variable which results from the interrelationship of strain partitioning and reaction progress. In our case, the proportion and arrangement of weak material with increasing strain first evolve into thin and polyphase shear bands, and then into connected broader high-strain zones (Fig. 14). We therefore conclude that the weakening of the samples is caused by the connectivity of the reaction products, giving rise to a bulk weakening that only achieves when the weak shear bands are interconnected.

4.5 Influence of deformation on reactions

One effect of deformation to solid-state chemical reactions is that deformation may enhance the kinetics of mineral reactions (e.g. Yund and Tullis, 1991; Wintsch et al., 1995; Baxter and De Paolo, 2004; Imon et al., 2002; Yonkee et al., 2003; Holyoke and Tullis, 2006; De Ronde and Stunitz, 2007, Richter et al., 2016). At the same time, mineral reactions enhance the nucleation rate, giving rise to very small grain sizes that favour the dominance of grain-size-sensitive creep (e.g. Rutter and Brodie, 1988; De Ronde et al., 2005; Marti et al., 2018). In our high-strain samples, we document a strong partitioning of deformation into high-strain zones (Fig. 4). The fact that the amount of reaction products increases with increasing strain at 850 and 900°C (Fig. 7a) strongly suggests that reaction kinetics are enhanced by deformation. Moreover, a higher amount of syn-kinematic amphiboles in high-strain zones indicates that the deformation-reaction feedback is pronounced, particularly in our “850 °C” sample. A similar feedback was found in sheared plagioclase-olivine experiments at 900°C (De Ronde and Stünitz, 2004, 2007), and they showed that the local strain is highly correlated with reaction progress. Recently, Marti et al., (2018) also described the positive feedback between deformation and reaction progress in experimentally deformed plagioclase-pyroxene mixtures, but in these examples, fewer reaction products have been described, probably due to the lower temperatures of their experiments. In addition, the greater reaction progress and larger amount of fine-grained mixed phase zones in our samples may be attributed to the small grain size of our starting material in otherwise very similar experimental procedures to Marti et al., (2018). The partially smaller grain size in our samples provides indeed a greater surface area of phase boundaries as sites of potential reactions.

Evidence of mineral reactions enhanced by deformation also arises from comparison between our hot-pressing, peak stress, and high-strain samples (Fig. 12a). The main difference between these samples is the bulk amount of reaction products. While hot-pressing and peak-stress samples both reveal a slight increase in the amount of reaction products with time (Fig. 12b), the high-strain samples produced far more reaction products for equivalent duration of experiment (Fig. 12b). Although two data points for hot-pressing samples are probably not enough to provide robust quantitative constraints, this reveals the strong influence of deformation on the amount of reaction products (Fig. 12b).

Similar results have been documented in experimentally deformed fine-grained gneiss (Holyoke and Tullis, 2006a; 2006b) and plagioclase + olivine samples (De Ronde and Stunitz, 2007). The main reason for the faster reaction progress in deformed samples is probably the introduction of defects into the reactants, i.e. the increase of the activation energy for the reaction at otherwise identical pressure and/or temperature overstepping conditions (De Ronde and Stunitz, 2007). Furthermore, the exposure of new reaction surfaces by grain boundary sliding can be another potentially important factor.

4.6 Geological implications – shear localization in nature

Several workers have pointed out that strain localization may control the degree of weakening in polyphase rocks (e.g. White et al., 1980; Handy, 1989), which is of great importance for the rheological behaviour of the lower crust. A large amount of fine-grained weak zones indeed allows to preserve the weak long-term behaviour of deep crustal rocks. It is also well established that the lower crust is lithologically heterogeneous, mainly consisting of mafic rocks dominated by feldspar and pyroxene (e.g. Kirby and Kronenberg, 1987; Christensen and Mooney, 1995; Rudnick and Fountain, 1995). However, current lithospheric models do not take into account the complex interaction between plagioclase and pyroxene on lower crust rheology. They do not either consider mechanical polyphase shear bands to describe the lower crust, yet observed in natural shear zones (e.g. Kanagawa et al., 2008; Kruse and Stünitz, 1999).

Mineral reaction and its interplay with deformation is of great importance for strain localization (e.g. Kerrich et al., 1980; Brodie and Rutter, 1985; Handy and Stünitz, 2002; Keller et al., 2004; Mansard et al., 2018). On one hand, cases of preserved metastable mineral assemblages in undeformed rocks are well documented, while deformed equivalents of the same rock body have significantly reacted (e.g. Austrheim and Griffin, 1985, Koons et al., 1987, Früh-Green, 1994). On the other hand, the extent of metamorphic reactions is greater in shear zones, as reaction may cause strain localization by producing a mechanically weak aggregate (Keller et al., 2004). In our experiments, the starting material made of Opx + Plag was deliberately chosen to be out of equilibrium at the experimental pressure and temperature conditions. Although large overstepping of reaction boundary probably occurred with respect to far slower changes of P-T conditions in nature, the experimental deformation of polyphase mixtures is here a good analogue to natural shear zones involving strain-enhanced chemical reactions and reaction-enhanced strain weakening.

In agreement with previous experiments (e.g. Rybacki and Dresen, 2000; Bystricky and Mackwell, 2001; Dimanov et al., 2003), our findings confirms that Opx + Plag assemblages are very strong, but as soon as these assemblages react, the material is viscously deformed and substantially weakened. The deformation of Opx + Plag assemblages also promoted diffusion-controlled chemical reactions, giving rise to the nucleation of new intrinsically strong phases, i.e., plagioclase and pyroxene (Fig. 2a). However, these strong phases nucleated as very fine grains within weak mixed phase zones (Fig. 6, 11), causing a switch in deformation mechanism, and thereby extending the range of conditions where fine-grained mixed zones are weaker than the unreacted assemblages. In addition, a critical parameter for the weakening to be effective is the connectivity of small weak zones at large scale. Our experiments demonstrate that the connectivity of weak material arises from feedbacks between deformation and phase reactions, causing a significant drop of the bulk sample strength, i.e., strain-induced weakening. The same effect may be therefore expected on a larger scale of the lower crust if small shear zones highly connect each other.

5. Conclusions

In this study, we have performed rock deformation experiments on plagioclase + pyroxene and pure end-member assemblages using the solid-medium Griggs-type apparatus at a pressure of 1 GPa and temperatures of 800, 850 and 900°C. The analysis of pure end-member assemblages reveals that 1) pure Opx deforms only by brittle mechanisms and 2) pure Plag deforms plastically at steady-state stress following a limited weakening after peak stress. In contrast, plagioclase + pyroxene assemblages show extensive strain-related weakening caused by mineral reactions. At the onset of deformation, new phases nucleate in aggregates as mixed phase tails and shear bands at the expense of original opx and plagioclase. The change of phase composition together with phase mixing indicates that grain size reduction originates from the consumption of reactants and nucleation of new phases. As deformation and reaction progress, the thin shear bands then coalesce to form highly connected material in the high-strain zones. Together with the occurrence of a significant weakening coeval with grain size reduction and phase mixing, our predictions suggest that shear bands deformed by grain-size-sensitive creep. The degree of connectivity, i.e. the formation of connected reacted material to a large extent, also played a major role in controlling the bulk sample strength. This highlights the importance of strain partitioning and shear bands connection to weaken shear zones. Providing analogue documentation of natural shear zones, our findings therefore emphasize the interactions between deformation and reaction to localize strain in ductile shear zones, particularly in mafic rocks.

Acknowledgements

This work has received funding from the European Research Council (ERC) under the seventh Framework Programme of the European Union (ERC Advanced Grant, grant agreement No 290864, RHEOLITH), and from the Labex VOLTAIRE (ANR-10-LABX-100-

01). The authors are grateful to Sylvain Janiec for the preparation of thin sections, Patricia Benoist and Ida Di-carlo for analytical support, Esteban Le Moing and Frédéric Savoie for technical assistance. We also thank Mark Zimmerman very much for kindly providing the Damaping peridotite material. The comments by an anonymous reviewer have improved the manuscript.

References

Austrheim, H., 1987. Eclogitization of lower crustal granulites by fluid migration through shear zones. Earth and Planetary Science Letters 81, 221–232. https://doi.org/10.1016/0012-821X(87)90158-0

Austrheim, H., Griffin, W.L., 1985. Shear deformation and eclogite formation within granulite-facies anorthosites of the Bergen Arcs, western Norway. Chemical Geology 50, 267–281. https://doi.org/10.1016/0009-2541(85)90124-X

Baxter, E.F., Depaolo, Æ.D.J., 2004. Can metamorphic reactions proceed faster than bulk strain ? 657–670. https://doi.org/10.1007/s00410-003-0525-3

Bercovici, D., Ricard, Y., 2012. Mechanisms for the generation of plate tectonics by two-phase grain-damage and pinning. Physics of the Earth and Planetary Interiors 202–203, 27–55. https://doi.org/10.1016/J.PEPI.2012.05.003

Berthé, D., Choukroune, P., Jegouzo, P., 1979. Orthogneiss, mylonite and non coaxial deformation of granites: the example of the South Armorican Shear Zone. Journal of Structural Geology 1, 31–42. https://doi.org/10.1016/0191-8141(79)90019-1

Boundy, T.M., Fountain, D.M., Austrheim, H., 1992. Structural development and petrofabrics of eclogite facies shear zones, Bergen Arcs, western Norway: implications for deep crustal deformational processes. Journal of Metamorphic Geology 10, 127–146. https://doi.org/10.1111/j.1525-1314.1992.tb00075.x

Brodie, K.H., 1980. Variations in mineral chemistry across a shear zone in phlogopite peridotite. Journal of Structural Geology 2, 265–272. https://doi.org/10.1016/0191-8141(80)90059-0

Brodie, K.H., Rutter, E.H., 1985. On the Relationship between Deformation and Metamorphism, with Special Reference to the Behavior of Basic Rocks. Springer, New

York, NY, 138–179. https://doi.org/10.1007/978-1-4612-5066-1_6

Bruijn, R., Skemer, P., 2014. Grain-size sensitive rheology of orthopyroxene. Geo-phys. Res. Lett. 41, 1–10. https://doi.org/10.1002/2014GL060607

Bürgmann, R., Dresen, G., 2008. Rheology of the Lower Crust and Upper Mantle: Evidence from Rock Mechanics, Geodesy, and Field Observations. Annual Review of Earth and Planetary Sciences 36, 531–567. https://doi.org/10.1146/annurev.earth.36.031207.124326

Burlini, L., Bruhn, D., 2005. High-strain zones: laboratory perspectives on strain softening during ductile deformation. Geological Society, London, Special Publications 245, 1–24. https://doi.org/10.1144/GSL.SP.2005.245.01.01

Bystricky, M., Lawlis, J., Mackwell, S., Heidelbach, F., Raterron, P., 2016. High-temperature deformation of enstatite aggregates. Journal of Geophysical Research: Solid Earth. 6384–6400. https://doi.org/10.1002/2016JB013011

Bystricky, M., Mackwell, S., 2001. Creep of dry clinopyroxene aggregates. Journal of Geophysical Research: Solid Earth 106, 13443–13454. https://doi.org/10.1029/2001JB000333

Chen, S., Hiraga, T., Kohlstedt, D.L., 2006. Water weakening of clinopyroxene in the dislocation creep regime. J. Geophys. Res. 111, B08203. https://doi.org/10.1029/2005JB003885

Chopra, P.N., Paterson, M.S., 1981. The experimental deformation of dunite. Tectonophysics 78, 453–473. https://doi.org/10.1016/0040-1951(81)90024-X

Christensen, N.I., Mooney, W.D., 1995. Seismic velocity structure and composition of the continental crust: A global view. Journal of Geophysical Research: Solid Earth 100, 9761–9788. https://doi.org/10.1029/95JB00259

De Bresser, J.H.P., Peach, C.J., Reijs, J.P.J., Spiers, C.J., 1998. On dynamic recrystallization during solid state flow: Effects of stress and temperature. Geophysical Research Letters 25, 3457–3460. https://doi.org/10.1029/98GL02690

De Bresser, J.H.P., Ter Heege, J.H., Spiers, C.J., 2001. Grain size reduction by dynamic recrystallization: Can it result in major rheological weakening? International Journal of Earth Sciences 90, 28–45. https://doi.org/10.1007/s005310000149

De Ronde, A.A., Heilbronner, R., Stünitz, H., Tullis, J., 2004. Spatial correlation of deformation and mineral reaction in experimentally deformed plagioclase–olivine aggregates. Tectonophysics 389, 93–109. https://doi.org/10.1016/J.TECTO.2004.07.054

De Ronde, A.A., Stünitz, H., Tullis, J., Heilbronner, R., 2005. Reaction-induced weakening of plagioclase–olivine composites. Tectonophysics 409, 85–106. https://doi.org/10.1016/J.TECTO.2005.08.008

De Ronde, A.A., Stunitz, H., 2007. Deformation-enhanced reaction in experimentally deformed plagioclase–olivine aggregates. Contributions to Mineralogy and Petrology 153, 699–717.

Dell'Angelo, L.N., Tullis, J., 1996. Textural and mechanical evolution with progressive strain in experimentally deformed aplite. Tectonophysics 256, 57–82. https://doi.org/10.1016/0040-1951(95)00166-2

Dimanov, A., Dresen, G., Xiao, X., Wirth, R., 1999. Grain boundary diffusion creep of synthetic anorthite aggregates: The effect of water. Journal of Geophysical Research: Solid Earth 104, 10483–10497. https://doi.org/10.1029/1998JB900113

Dimanov, A., Dresen, G., 2005. Rheology of synthetic anorthite-diopside aggregates: Implications for ductile shear zones. Journal of Geophysical Research 110, B07203. https://doi.org/10.1029/2004JB003431

Dimanov, A., Lavie, M.P., Dresen, G., Ingrin, J., Jaoul, O., 2003. Creep of polycrystalline anorthite and diopside. Journal of Geophysical Research: Solid Earth 108. https://doi.org/10.1029/2002JB001815

Dimanov, A., Rybacki, E., Wirth, R., Dresen, G., 2007. Creep and strain-dependent microstructures of synthetic anorthite–diopside aggregates. Journal of Structural Geology 29, 1049–1069. https://doi.org/10.1016/J.JSG.2007.02.010

Etheridge, M.A., Wilkie, J.C., 1979. Grainsize reduction, grain boundary sliding and the flow strength of mylonites. Tectonophysics 58, 159–178. https://doi.org/10.1016/0040-1951(79)90327-5

Fitz Gerald, J., Stünitz, H., 1993. Deformation of granitoids at low m~tamo~~ic grade. I: Reactions and grain size reduction. Elsevier Science Publishers B.V 221, 269–297. https://doi.org/10.1016/0040-1951(93)90164-F

Fliervoet, T.F., White, S.H., Drury, M.R., 1997. Evidence for dominant grain-boundary sliding deformation in greenschist- and amphibolite-grade polymineralic ultramylonites from the Redbank Deformed Zone, Central Australia. Journal of Structural Geology 19, 1495–1520. https://doi.org/10.1016/S0191-8141(97)00076-X

Früh-Green, G.L., 1994. Interdependence of deformation, fluid infiltration and reaction progress recorded in eclogitic metagranitoids (Sesia Zone, Western Alps). Journal of Metamorphic Geology 12, 327–343. https://doi.org/10.1111/j.1525-1314.1994.tb00026.x

Gapais, D., 1989. Shear structures within deformed granites: mechanical and thermal indicators. Geology 17, 1144–1147. https://doi.org/10.1130/0091-7613(1989)017<1144:SSWDGM>2.3.CO

Gerbi, C., Johnson, S.E., Shulman, D., Klepeis, K., 2016. Influence of microscale weak zones on bulk strength. Geochemistry, Geophysics, Geosystems 17, 4064–4077. https://doi.org/10.1002/2016GC006551

Gerya, T., 2010. Introduction to Numerical Geodynamic Modelling. Cambridge University Press, ISBN 9780521887540.

Gerya, T. V., Stöckhert, B., Perchuk, A.L., 2002. Exhumation of high-pressure metamorphic rocks in a subduction channel: A numerical simulation. Tectonics 21, 6-1-6–19. https://doi.org/10.1029/2002TC001406

Getsinger, A.J., Hirth, G., 2014. Amphibole fabric formation during diffusion creep and the rheology of shear zones. 535–538. https://doi.org/10.1130/G35327.1

Glodny, J., Austrheim, H., Molina, J.F., Rusin, A.I., Seward, D., 2003. Rb/Sr record of fluid-rock interaction in eclogites: The Marun-Keu complex, Polar Urals, Russia. Geochimica et Cosmochimica Acta 67, 4353–4371. https://doi.org/10.1016/S0016-7037(03)00370-3

Gueydan, F., Précigout, J., Montési, L.G.J., 2014. Strain weakening enables continental plate tectonics. Tectonophysics 631, 189–196. https://doi.org/10.1016/J.TECTO.2014.02.005

Handy, M.R., 1994. Flow laws for rocks containing two non-linear viscous phases: A phenomenological approach. Journal of Structural Geology 16, 287–301. https://doi.org/10.1016/0191-8141(94)90035-3

Handy, M.R., 1990. The solid-state flow of polymineralic rocks. Journal of Geophysical Research 95, 8647. https://doi.org/10.1029/JB095iB06p08647

Handy, M.R., 1989. Deformation regimes and the rheological evolution of fault zones in the lithosphere: the effects of pressure, temperature, grainsize and time. Tectonophysics 163, 119–152. https://doi.org/10.1016/0040-1951(89)90122-4

Handy, M.R., Stünitz, H., 2002. Strain localization by fracturing and reaction weakening — a mechanism for initiating exhumation of subcontinental mantle beneath rifted margins. Geological Society, London, Special Publications 200, 387–407. https://doi.org/10.1144/GSL.SP.2001.200.01.22

Hansen, L.N., Zimmerman, M.E., Dillman, A.M., Kohlstedt, D.L., 2012. Strain localization in olivine aggregates at high temperature: A laboratory comparison of constant-strain-rate and constant-stress boundary conditions. Earth and Planetary Science Letters 333–334, 134–145. https://doi.org/10.1016/J.EPSL.2012.04.016

Heilbronner, R, Barrett, S., 2014. Image Analysis. In: Image Analysis in Earth Sciences. Springer Heidelberg, Berlin, Heidelberg, pp 137–156. https://doi.org/10.1007/978-3-642-10343-8_1.

Heilbronner, R., 2002. Analysis of bulk fabrics and microstructure variations using tesselations of autocorrelation functions. Computers & Geosciences 28, 447–455. https://doi.org/10.1016/S0098-3004(01)00088-7

Heilbronner, R.P., 1992. The autocorrelation function: an image processing tool for fabric analysis. Tectonophysics 212, 351–370. https://doi.org/10.1016/0040-1951(92)90300-U

Herwegh, M., Linckens, J., Ebert, A., Berger, A., Brodhag, S.H., 2011. The role of second phases for controlling microstructural evolution in polymineralic rocks: A review. Journal of Structural Geology 33, 1728–1750. https://doi.org/10.1016/j.jsg.2011.08.011

Hidas, K., Tommasi, A., Garrido, C.J., Padrón-Navarta, J.A., Mainprice, D., Vauchez, A., Barou, F., Marchesi, C., 2016. Fluid-assisted strain localization in the shallow subcontinental lithospheric mantle. Lithos 262, 636–650. https://doi.org/10.1016/j.lithos.2016.07.038

Hirth, G., Tullis, J., 1992. Dislocation creep regimes in quartz aggregates. Journal of Structural Geology 14, 145–159. https://doi.org/10.1016/0191-8141(92)90053-Y

Holyoke, C.W., Tullis, J., 2006a. Mechanisms of weak phase interconnection and the effects of phase strength contrast on fabric development. Journal of Structural Geology 28, 621–

640. https://doi.org/10.1016/j.jsg.2006.01.008

Holyoke, C.W., Tullis, J., 2006b. Formation and maintenance of shear zones. Geology 34, 105–108. https://doi.org/10.1130/G22116.1

Imon, R., Okudaira, T., Fujimoto, A., 2002. Dissolution and precipitation processes in deformed amphibolites: an example from the ductile shear zone of the Ryoke metamorphic belt, SW Japan. Journal of Metamorphic Geology 20, 297–308. https://doi.org/10.1046/j.1525-1314.2002.00367.x

Jamtveit, B., Austrheim, H., Putnis, A., 2016. Disequilibrium metamorphism of stressed lithosphere. Earth-Science Reviews 154, 1–13. https://doi.org/10.1016/J.EARSCIREV.2015.12.002

Jordan, P., 1988. The rheology of polymineralic rocks - an approach. Geologische Rundschau 77, 285–294. https://doi.org/10.1007/BF01848690

Kanagawa, K., Shimano, H., Hiroi, Y., 2008. Mylonitic deformation of gabbro in the lower crust: A case study from the Pankenushi gabbro in the Hidaka metamorphic belt of central Hokkaido, Japan. Journal of Structural Geology 30, 1150–1166. https://doi.org/10.1016/j.jsg.2008.05.007

Keller, L.M., Abart, R., Stünitz, H., De Capitani, C., 2004. Deformation, mass transfer and mineral reactions in an eclogite facies shear zone in a polymetamorphic metapelite (Monte Rosa nappe, western Alps). Journal of Metamorphic Geology 22, 97–118. https://doi.org/10.1111/j.1525-1314.2004.00500.x

Kenkmann, T., Dresen, G., 2002. Dislocation microstructure and phase distribution in a lower crustal shear zone - An example from the Ivrea-Zone, Italy. International Journal of Earth Sciences 91, 445–458. https://doi.org/10.1007/s00531-001-0236-9

Kerrich, R., Allison, I., Barnett, R.L., Moss, S., Starkey, J., 1980. Microstructural and chemical transformations accompanying deformation of granite in a shear zone at Mi??ville, Switzerland; with implications for stress corrosion cracking and superplastic flow. Contributions to Mineralogy and Petrology 73, 221–242. https://doi.org/10.1007/BF00381442

Kilian, R., Heilbronner, R., Stünitz, H., 2011. Quartz grain size reduction in a granitoid rock and the transition from dislocation to diffusion creep. Journal of Structural Geology 33, 1265–1284. https://doi.org/10.1016/j.jsg.2011.05.004

Kirby, S.H., Kronenberg, A.K., 1987. Rheology of the lithosphere: Selected topics. Reviews of Geophysics 25, 1219. https://doi.org/10.1029/RG025i006p01219

Kohlstedt, D.L., Evans, B., Mackwell, S.J., 1995. Strength of the lithosphere: Constraints imposed by laboratory experiments. Journal of Geophysical Research: Solid Earth 100, 17587–17602. https://doi.org/10.1029/95JB01460

Koons, P.O., Rubie, D.C., Fruch-Green, G., 1987. The Effects of Disequilibrium and Deformation on the Mineralogical Evolution of Quartz Diorite During Metamorphism in the Eclogite Facies. Journal of Petrology 28, 679–700. https://doi.org/10.1093/petrology/28.4.679

Kruse, R., Stünitz, H., 1999. Deformation mechanisms and phase distribution in mafic high-temperature mylonites from the Jotun Nappe, southern Norway. Tectonophysics 303, 223–249. https://doi.org/10.1016/S0040-1951(98)00255-8

Langdon, T.G., 2006. Grain boundary sliding revisited: Developments in sliding over four decades. Journal of Materials Science 41, 597–609. https://doi.org/10.1007/s10853-006-6476-0

Linckens, J., Bruijn, R.H.C., Skemer, P., 2014. Dynamic recrystallization and phase mixing in experimentally deformed peridotite. Earth and Planetary Science Letters 388, 134–142. https://doi.org/10.1016/J.EPSL.2013.11.037

Linckens, J., Herwegh, M., Mntener, O., Mercolli, I., 2011. Evolution of a polymineralic mantle shear zone and the role of second phases in the localization of deformation. Journal of Geophysical Research: Solid Earth 116, 1–21. https://doi.org/10.1029/2010JB008119

Mansard, N., Raimbourg, H., Augier, R., Précigout, J., Le Breton, N., 2018. Large-scale strain localization induced by phase nucleation in mid-crustal granitoids of the south Armorican massif. Tectonophysics 745, 46–65. https://doi.org/10.1016/j.tecto.2018.07.022

Marti, S., Stünitz, H., Heilbronner, R., Plümper, O., Drury, M., 2017. Experimental investigation of the brittle-viscous transition in mafic rocks – Interplay between fracturing, reaction, and viscous deformation. Journal of Structural Geology 105, 62–79.

https://doi.org/10.1016/j.jsg.2017.10.011

Marti, S., Stünitz, H., Heilbronner, R., Plümper, O., Kilian, R., 2018. Syn-kinematic hydration reactions , grain size reduction , and dissolution – precipitation creep in experimentally deformed plagioclase – pyroxene mixtures. 985–1009. https://doi.org/10.5194/se-9-985-2018

Menegon, L., Fusseis, F., Stünitz, H., Xiao, X., 2015. Creep cavitation bands control porosity and fluid flow in lower crustal shear zones. Geology 43, 227–230. https://doi.org/10.1130/G36307.1

Mitra, G., 1978. Ductile deformation zones and mylonites; the mechanical processes involved in the deformation of crystalline basement rocks. American Journal of Science 278, 1057–1084. https://doi.org/10.2475/ajs.278.8.1057

Montési, L.G.J., 2013. Fabric development as the key for forming ductile shear zones and enabling plate tectonics. Journal of Structural Geology 50, 254–266. https://doi.org/10.1016/j.jsg.2012.12.011

Montési, L.G.J., 2007. A constitutive model for layer development in shear zones near the brittle-ductile transition. Geophysical Research Letters 34, 1–5. https://doi.org/10.1029/2007GL029250

Newman, J., Lamb, W.M., Drury, M.R., Vissers, R.L.M., 1999. Deformation processes in a peridotite shear zone: reaction-softening by an H2O-deficient, continuous net transfer reaction. Tectonophysics 303, 193–222. https://doi.org/10.1016/S0040-1951(98)00259-5

Newman, J., Mitra, G., 1993. Lateral variations in mylonite zone thickness as influenced by fluid-rock interactions, Linville falls fault, North Carolina. Journal of Structural Geology 15, 849–863. https://doi.org/10.1016/0191-8141(93)90180-I

Olgaard, D.L., 1990. The role of second phase in localizing deformation. Geological Society, London, Special Publications 54, 175–181. https://doi.org/10.1144/GSL.SP.1990.054.01.17

Palazzin, G., Raimbourg, H., Stünitz, H., Heilbronner, R., Neufeld, K., Précigout, J., 2018. Evolution in H2O contents during deformation of polycrystalline quartz: An experimental study. Journal of Structural Geology 114, 95–110. https://doi.org/10.1016/J.JSG.2018.05.021

Panozzo, R., 1983. Two-dimensional analysis of shape-fabric using projections of digitized lines in a plane. Tectonophysics 95, 279–294. https://doi.org/10.1016/0040-1951(83)90073-2

Park, Y., Yoo, S.H., Ree, J.H., 2006. Weakening of deforming granitic rocks with layer development at middle crust. Journal of Structural Geology 28, 919–928. https://doi.org/10.1016/j.jsg.2006.02.005

Paterson, M.S., Luan, F.C., 1990. Quartzite rheology under geological conditions. Geological Society, London, Special Publications 54, 299–307. https://doi.org/10.1144/GSL.SP.1990.054.01.26

Paterson, M. S., 2013. Materials science for structural geology, Springer Dordrecht Heidelberg New York London, p. 247, doi:10.1007/978-94-007-5545-1

Pec, M., Stünitz, H., Heilbronner, R., 2012. Semi-brittle deformation of granitoid gouges in shear experiments at elevated pressures and temperatures. 38. https://doi.org/10.1016/j.jsg.2011.09.001

Pec, M., Stünitz, H., Heilbronner, R., Drury, M., 2016. Semi-brittle flow of granitoid fault rocks in experiments. Journal of Geophysical Research: Solid Earth 121, 1677–1705. https://doi.org/10.1002/2015JB012513

Platt, J.P., 2015. Rheology of two-phase systems: A microphysical and observational approach. Journal of Structural Geology 77, 213–227. https://doi.org/10.1016/j.jsg.2015.05.003

Poirier, J.P., 1980. Shear localization and shear instability in materials in the ductile field. Journal of Structural Geology 2, 135–142. https://doi.org/10.1016/0191-8141(80)90043-7

Precigout, J., Gueydan, F., Gapais, D., Garrido, C.J., Essaifi, A., 2007. Strain localisation in the subcontinental mantle — a ductile alternative to the brittle mantle. Tectonophysics 445, 318–336. https://doi.org/10.1016/J.TECTO.2007.09.002

Précigout, J., Stünitz, H., 2016. Evidence of phase nucleation during olivine diffusion creep: A new perspective for mantle strain localisation. Earth and Planetary Science Letters 455, 94–105. https://doi.org/10.1016/j.epsl.2016.09.029

Précigout, J., Stünitz, H., Pinquier, Y., Champallier, R., Schubnel, A., 2018. High-pressure, High-temperature Deformation Experiment Using the New Generation Griggs-type Apparatus. Journal of Visualized Experiments : JoVE. https://doi.org/10.3791/56841

Précigout, J., Prigent, C., Palasse, L., Pochon, A., 2017. Water pumping in mantle shear zones. Nature communications 8: 15736, https://doi.org/10.1038/ncomms15736

Précigout, J., Stünitz, H., Villeneuve, J., 2019. Excess water storage induced by viscous strain localization during high-pressure shear experiment. Scientific Reports 9: 3463, httpx://doi.org/10.1038/s41598-019-40020-y.

Prigent, C., Guillot, S., Agard, P., Lemarchand, D., Soret, M., Ulrich, M., 2018. Transfer of subduction fluids into the deforming mantle wedge during nascent subduction: Evidence from trace elements and boron isotopes (Semail ophiolite, Oman). Earth and Planetary Science Letters 484, 213–228. https://doi.org/10.1016/J.EPSL.2017.12.008

Raimbourg, H., Toyoshima, T., Harima, Y., Kimura, G., 2008. Grain-size reduction mechanisms and rheological consequences in high-temperature gabbro mylonites of Hidaka, Japan. Earth and Planetary Science Letters 267, 637–653. https://doi.org/10.1016/j.epsl.2007.12.012

Ramsay, J.G., 1980. Shear zone geometry: A review. Journal of Structural Geology 2, 83–99. https://doi.org/10.1016/0191-8141(80)90038-3

Ree, J.H., Kim, H.S., Han, R., Jung, H., 2005. Grain-size reduction of feldspars by fracturing and neocrystallization in a low-grade granitic mylonite and its rheological effect. Tectonophysics 407, 227–237. https://doi.org/10.1016/j.tecto.2005.07.010

Richter, B., Stünitz, H., Heilbronner, R., 2016. Stresses and pressures at the quartz-to-coesite phase transformation in shear deformation experiments. Journal of Geophysical Research: Solid Earth 121, 8015–8033. https://doi.org/10.1002/2016JB013084

Richter, B., Stünitz, H., & Heilbronner, R. (2018). The brittle-to-viscous transition in polycrystalline quartz: An experimental study. Journal of Structural Geology, 114, 1-21. https://doi.org/10.1016/j.jsg.2018.06.005

Rosenberg, C.L., Handy, M.R., 2005. Experimental deformation of partially melted granite revisited: implications for the continental crust. Journal of Metamorphic Geology 23, 19–28. https://doi.org/10.1111/j.1525-1314.2005.00555.x

Rudnick, R.L., Fountain, D.M., 1995. Nature and composition of the continental crust: A lower crustal perspective. Reviews of Geophysics 33, 267. https://doi.org/10.1029/95RG01302

Rutter, E.H., Brodie, K.H., 1988a. The role of tectonic grain size reduction in the rheological stratification of the lithosphere. Geologische Rundschau 77, 295–307. https://doi.org/10.1007/BF01848691

Rybacki, E., Dresen, G., 2000. Dislocation and diffusion creep of synthetic anorthite aggregates. Journal of Geophysical Research: Solid Earth 105, 26017–26036. https://doi.org/10.1029/2000JB900223

Schmid, S.M., Paterson, M.S., Boland, J.N., 1980. High temperature flow and dynamic recrystallization in carrara marble. Tectonophysics 65, 245–280. https://doi.org/10.1016/0040-1951(80)90077-3

Schmid, S.M., 1982. Microfabric studies as Indicators of Deformation Mechanisms and Flow Laws Operative in Mountain Building. In: Hsü, K.J. (Ed.), Mountain Building Processes. Academic Press, pp. 95e110.

Stünitz, H., Fitz Gerald, J.D., 1993. Deformation of granitoids at low metamorphic grades: II. Granular flow in albite rich mylonites. Tectonophysics 221, 299–324. https://doi.org/10.1016/0040-1951(93)90164-F

Stünitz, H., Tullis, J., 2001. Weakening and strain localization produced by syn-deformational reaction of plagioclase. International Journal of Earth Sciences 90, 136–148. https://doi.org/10.1007/s005310000148

Tackley, P.J., 1998. Self-consistent generation of tectonic plates in three-dimensional mantle convection. Earth and Planetary Science Letters 157, 9–22. https://doi.org/10.1016/S0012-821X(98)00029-6

Tarantola, A., Diamond, L., Stünitz, H., 2010. Modification of fluid inclusions in quartz by deviatoric stress I: experimentally induced changes in inclusion shapes and microstructures. Contributions to Mineralogy and Petrology 160 (6), 825–843. doi:10.1007/s00410-010-0509-z.

Tasaka, M., Zimmerman, M. E., Kohlstedt, D. L., Stünitz, H., & Heilbronner, R. (2017). Rheological weakening of olivine+ orthopyroxene aggregates due to phase mixing: Part 2. Microstructural development. Journal of Geophysical Research: Solid Earth, 122(10), 7597-7612.

Tokle, L., Hirth, G., Behr, W.M., 2019. Flow laws and fabric transitions in wet quartzite. Earth and Planetary Science Letters 505, 152–161. https://doi.org/10.1016/J.EPSL.2018.10.017

Tullis, J., Yund, R.A., 1985. Dynamic recrystallisation of feldspar: a mechanism for ductile shear zone formation. Geology 13, 238–241. https://doi.org/10.1130/0091-7613(1985)13<238:DROFAM>2.0.CO;2

Viegas, G., Menegon, L., Archanjo, C., 2016. Brittle grain-size reduction of feldspar, phase mixing and strain localization in granitoids at mid-crustal conditions (Pernambuco shear zone, NE Brazil). Solid Earth 7, 375–396. https://doi.org/10.5194/se-7-375-2016

Wassmann, S., Stöckhert, B., 2013. Rheology of the plate interface - dissolution precipitation creep in high pressure metamorphic rocks. Tectonophysics 608, 1–29. https://doi.org/10.1016/j.tecto.2013.09.030

Weaver, B.L., Tarney, J., 1984. Major and trace element composition of the continental lithosphere. Physics and Chemistry of the Earth 15, 39–68. https://doi.org/10.1016/0079-1946(84)90004-1

White, S.H., Burrows, S.E., Carreras, J., Shaw, N.D., Humphreys, F.J., 1980. On mylonites in ductile shear zones. Journal of Structural Geology 2, 175–187. https://doi.org/10.1016/0191-8141(80)90048-6

Whitmeyer, S.J., Wintsch, R.P., 2005. Reaction localization and softening of texturally hardened mylonites in a reactivated fault zone, central Argentina. Journal of Metamorphic Geology 23, 411–424. https://doi.org/10.1111/j.1525-1314.2005.00588.x

Wintsch, R.P., Christoffersen, R., Kronenberg, A.K., 1995. Fluid-rock reaction weakening of fault zones. Journal of Geophysical Research: Solid Earth 100, 13021–13032. https://doi.org/10.1029/94JB02622

Yonkee, W.A., Parry, W.T., Bruhn, R.L., 2003. Relations between progressive deformation and fluid-rock interaction during shear-zone growth in a basement-cored thrust sheet, Sevier orogenic belt, Utah. American Journal of Science 303, 1–59. https://doi.org/10.2475/ajs.303.1.1

Yund, R.A., Tullis, J., 1991. Compositional changes of minerals associated with dynamic recrystallizatin. Contributions to Mineralogy and Petrology 108, 346–355. https://doi.org/10.1007/BF00285942

Figure Captions

Fig. 1. Sample assembly of the shear experiments using a Griggs-type apparatus. **a**) Schematic cross-section of the assembly in a new generation Griggs rig at the University of Orléans (France). **b**) Schematic drawing of sample geometry in a 3D view. Sample powder is inserted between 45° pre-cut alumina forcing blocks. Modified after Tarantola et al., 2010. **c**) Sample geometry at the end of the experiment: th_0 = initial thickness, th_f = final thickness.

Fig. 2. Differential stress (MPa) versus shear strain (γ) plots. **a**) Set of terms used to describe the mechanical data. **b**) Stress-strain curves showing the mechanical behaviour of two pure plagioclase samples deformed at 800 and 900 °C. The mechanical curve of a pure pyroxene sample deformed at 900 °C with an initial coarser grain size (< 40 µm) is also plotted. **c-d**) Set of experiments deforming an Opx + Plag mixture at different temperatures (800, 850 and 900°C), and at constant confining pressure, strain rate and water content. These experiments are separated in two graphs according to the different duration of the "run-in" section. The colour coding refers to the temperature of the experiments.

Fig. 3. SEM-BSE images representative of microstructures documented in pure plagioclase (**a**) and pyroxene (**b-c**) experiments. **a**) Plagioclase grain size refinement (blue arrows) by dynamic recrystallization. **b**) Fractures in pyroxene grains. **c**) Close-up of the pyroxene grains showing local extensive grain size refinement in cracks (orange arrows). pl = plagioclase.

Fig. 4. SEM-BSE images across of the high-shear-strain sample (**a**) and related phase map digitized manually (**b**), showing the overall strain gradient in the shear zone from top to bottom. This transect is characterized by a heterogeneity in the amount of reaction and deformation. rp = reaction products, opx = orthopyroxene, cpx = clinopyroxene, pl = plagioclase, amph = amphibole, alumina FB = alumina forcing block.

Fig. 5. SEM-BSE images representative of microstructures observed in the high-shear-strain experiments. **a-b**) The reaction products appear as coronas around the original Opx_1 and as aggregates in low-strain zones. Pyroxene is locally fractured and filled with reaction products (white arrows). **c-d**) The transition zone shows the development of fine-grained tails and shear bands extending at the edges of Opx_1. These tails form fine-grained mixed zones rich in Opx_2, Pl_2 and Amph. **e-f**) High-strain zones textures are made of intercalated fine-grained polyphase shear bands. In these zones, an extensive phase mixing between Opx_2, Pl_2 and Amph is observed. The original Pl_1 almost completely disappears, while some Opx_1 clasts, which are reduced in size, remains within these fine-grained mixed zones. opx = orthopyroxene, cpx = clinopyroxene, pl = plagioclase, amph = amphibole, qtz = quartz.

Fig. 6. SEM-BSE images representative of microstructures observed in the high-strain zones. Three samples deformed to high shear strain are documented: one deformed at 850°C (**a-b**) and two others deformed at 900°C (**c-d-e**). In each case, the high-strain zones are made of fine-grained polyphase shear bands, mainly composed of Opx_2, Pl_2 and Amph. However, the volume fraction of reaction products is larger at 850°C and the deformation is more localized compared to samples deformed at 900°C, which show more distributed deformation and lower amounts of amphiboles at the scale of the shear zone. Opx = orthopyroxene, cpx = clinopyroxene, pl = plagioclase, amph = amphibole, qtz = quartz.

Fig. 7. Analysis of the phase content (a), aspect ratio (b-c) and shape preferred orientation (d) across the high-shear-strain sample shown in Figure 4. For reference, panel (**a**) shows the evolution of phases as volume fraction through the transect. Opx_2 and Amph as reaction products are grouped together. Panel (**b**) displays the bulk aspect ratio R*, while the panel (**c**) displays the aspect ratio R* for individual phases. Panel (**d**) shows the preferred orientation of angle α* of the bulk fabric with respect to the piston interfaces. While the amount of reaction products is higher in the high-strain zone compared to low-strain ones, the ACF analysis reveals a higher aspect ratio of the fabric in the high-strain zones, essentially of the reaction products, which are preferentially oriented subparallel to the piston interfaces. Opx = orthopyroxene, cpx = clinopyroxene, pl = plagioclase, amph = amphibole.

Fig. 8. Chemical composition of plagioclase (**a**), pyroxene (**b**), and amphibole (**c**). The chemical compositions of plagioclase and pyroxene are divided into three subsets: clast-core, clast-rim and fine grains. The frequency corresponds to the number of grains analysed considering one point per grain.

Fig. 9. SEM-BSE images representative of microstructures observed in the hot-pressing experiments (**a-b-c**) and peak stress experiments (**d-e**). **a-b**) Thin reaction coronas that start forming at the Opx_1-Pl_1 interphase boundaries. This consists essentially of Opx_2 and $Plag_2$. **c**) Aggregate of original Opx_1 replaced by Opx_2. **d**) Representative microstructures observed at peak stress where the reaction products start to form aggregates that are partially connected in the direction of extension. **e**) Irregular grain boundaries composed of small grains of newly formed reaction products. Opx = orthopyroxene, cpx = clinopyroxene, pl = plagioclase, amph = amphibole.

Fig. 10. SEM-BSE images showing characteristic microstructures of the nascent mixing of phases. **a**) Incipient interconnection of thin shear bands filled with fine-grained polyphase mixture (yellow dotted outline) subparallel to the shear plane (horizontal direction). **b**) Close-up of shear bands showing fine-

grained mixture of Opx_2, Pl_2 and Amph. **c**) Close-up of incipient mixing forming tails at the edges of original Opx_1. Opx = orthopyroxene, cpx = clinopyroxene, pl = plagioclase, amph = amphibole.

Fig. 11. Grain size evolution of pyroxene between peak-stress experiment (mode: 15.6 µm; mean: 15.3 µm) and the newly formed Opx_2 in fine-grained mixed zones in high-shear-strain experiments (mode: 0.2 µm; mean: 0.4 µm). The black curve represents a best-fit to the log-normal distribution. The average value for the aspect ratio of new Opx grains is a/b = 1.23.

Fig. 12. Evolution of the amount of reaction products as a function of time in plagioclase – pyroxene experiments at 900°C. Symbols denote types of experiments performed, which include hot-pressing, peak-stress, intermediate and high-shear-strain experiments. The graph in (**a**) shows the different types of experiments, strain rate and associated mechanical data in stress-strain graph. **b**) Evolution of the volume fraction of reaction products (RP) with time, and effect of deformation on reaction and sample strength. Avrami curve fitting for hot-pressed or deformed samples are colour coded. One curve for deformed samples is fitted for peak-stress samples, while the other is fitted for higher-shear-strain samples. The duration of the deformed experiments is taken from the hit-point.

Fig. 13. Deformation mechanism map for dry orthopyroxene (**a**), wet clinopyroxene (**b**) and wet plagioclase (**c**) at 900°C and 1 GPa. On these maps, we plot the differential stress and grain size of Opx at peak-stress conditions and in mixed zones of high-shear-strain experiments in both cases, as we consider that the grain size of plagioclase and pyroxene is similar. The deformation conditions of the pure Plag sample is also plotted. The grain size is represented in box-and-whisker diagram that includes the median (white lines), mean (green lines) and mode (blue lines). The flow laws are from Bruijn and Skemer, 2014 and Bystricky et al., 2016 for dry orthopyroxene, from Dimanov and Dresen

(2005) for wet clinopyroxene and from Rybacki and Dresen (2000) for wet plagioclase. The grain size piezometer for Opx (yellow line) is taken from the study of Linckens et al. (2014).

Fig. 14. Schematic textural and microstructural evolution of plagioclase-pyroxene mixture from hot-pressing conditions (**A**) through peak-stress conditions (**B**) to strongly deformed shear zones (**C**). This figure illustrates the different stages of strain localization and weakening during deformation.

Tables

Table. 1. Composition of plagioclase (Plag) and orthopyroxene (Opx) as starting material.

Table. 2. Summary of experimental conditions. Type: HP - hot-pressing, PS: peak stress, D: deformed samples to varying amounts of shear strain. A cross marks is added to the type of deformation when the forcing blocks started to slip at the sample interface; τ_{peak}: differential stress at peak, τ_{flow}: steady-state differential stress, τ_{end}: differential stress at end of experiment, γ: shear strain, th_0: thickness initial of the shear zone, thf: final shear zone thickness.

Table. 3. Representative chemical composition of plagioclase, orthopyroxene and amphibole.

Table. 1.

	Sonora labradorite		**Damaping Mg-Opx**	
	Wt. % oxides	Atoms per 8 oxygen	Wt. % oxides	Atoms per 6 oxygen
SiO_2	53,87	2,434	55,71	1,929
Al_2O_3	29,41	1,566	3,81	0,155
CaO	11,68	0,565	0,42	0,016
Na_2O	4,06	0,356	0,07	0,005
K_2O	0,46	0,027	0,02	0,001
MgO	0,09	0,006	32,51	1,678
TiO_2	0,08	0,003	0,07	0,002
FeO	0,38	0,014	7,21	0,209
MnO	0,05	0,002	0,18	0,005
Total	100,08	4,972	100,01	4,000
	An60 **Ab**38 **Or**2		**Wo**1 **En**88 **Fs**11	

Table. 2.

Exp. Nr	Material	Type	T	P	H_2O	τ_{peak}	τ_{flow}	τ_{end}	γ	th0	thf
			[°C]	[GPa]	µL	[MPa]	[MPa]	[MPa]		[mm]	[mm]
535NM	Plag	D	900	1	0,12	620	524	524	2,9	0,75	0,57
537NM	Opx	PS	900	1	0,12	1600	-	1546	0,9	0,75	0,69
557NM	Opx + Plag	PS^x	850	1	0,12	1067	-	577	0,4	0,75	0,59
559NM	Opx + Plag	PS^x	800	1	0,12	1111	-	350	0,5	0,75	0,67
OR24NM	Opx + Plag	D^x	800	1	0,25	1280	-	866	3,1	1,1	0,87
OR34NM	Opx + Plag	D	900	1	0,25	781	114	126	7,6	1,1	0,68
OR38NM	Opx + Plag	D	850	1	0,25	1038	339	339	8,0	1,1	0,63
OR41NM	Opx + Plag	D	900	1	0,25	1094	542	542	7,0	1,1	0,72
OR43NM	Opx + Plag	HP	900	1	0,25	-	-	-	-	1,1	1,1
OR47NM	Opx + Plag	PS	900	1	0,25	989	-	989	0,6	1,1	0,91
OR49NM	Opx + Plag	D^x	900	1	0,25	1111	800	800	6,0	1,1	0,73
OR51NM	Opx + Plag	PS	900	1	0,25	901	-	901	0,8	1,1	1
OR53NM	Plag	D	800	1	0,25	904	746	746	4,7	1,1	1
OR55NM	Opx + Plag	HP	900	1	0,25	-	-	-	-	1,1	1,1

Table. 3.

	Plagioclase			Orthopyroxene			Amphibole
	Core	Rim	Fine-grains	Core	Rim	Fine-grains	
SiO_2	54,70	55,35	55,10	55,48	55,57	55,77	49,82
Al_2O_3	30,89	28,99	29,50	3,91	4,62	5,63	10,62
CaO	10,24	9,90	9,65	1,03	1,14	1,13	12,50
Na_2O	3,87	4,97	5,51	0,24	0,01	0,10	2,10
K_2O	0,14	0,28	0,25	0,03	0,02	0,03	0,00
MgO	0,07	0,22	0,04	32,04	30,29	27,90	19,22
TiO_2	0,13	0,04	0,00	0,06	0,07	0,08	0,21
FeO	0,13	0,16	0,04	7,17	8,40	9,75	3,61
MnO	0,00	0,02	0,05	0,07	0,03	0,05	0,00
Total	100,17	99,93	100,14	100,03	100,14	100,43	98,08
	An59 **Ab**40 **Or**1	**An**52 **Ab**47 **Or**1	**An**49 **Ab**50 **Or**1	**Wo**2 **En**87 **Fs**11	**Wo**2 **En**84 **Fs**13	**Wo**2 **En**81 **Fs**16	**Magnesio-hornblende**

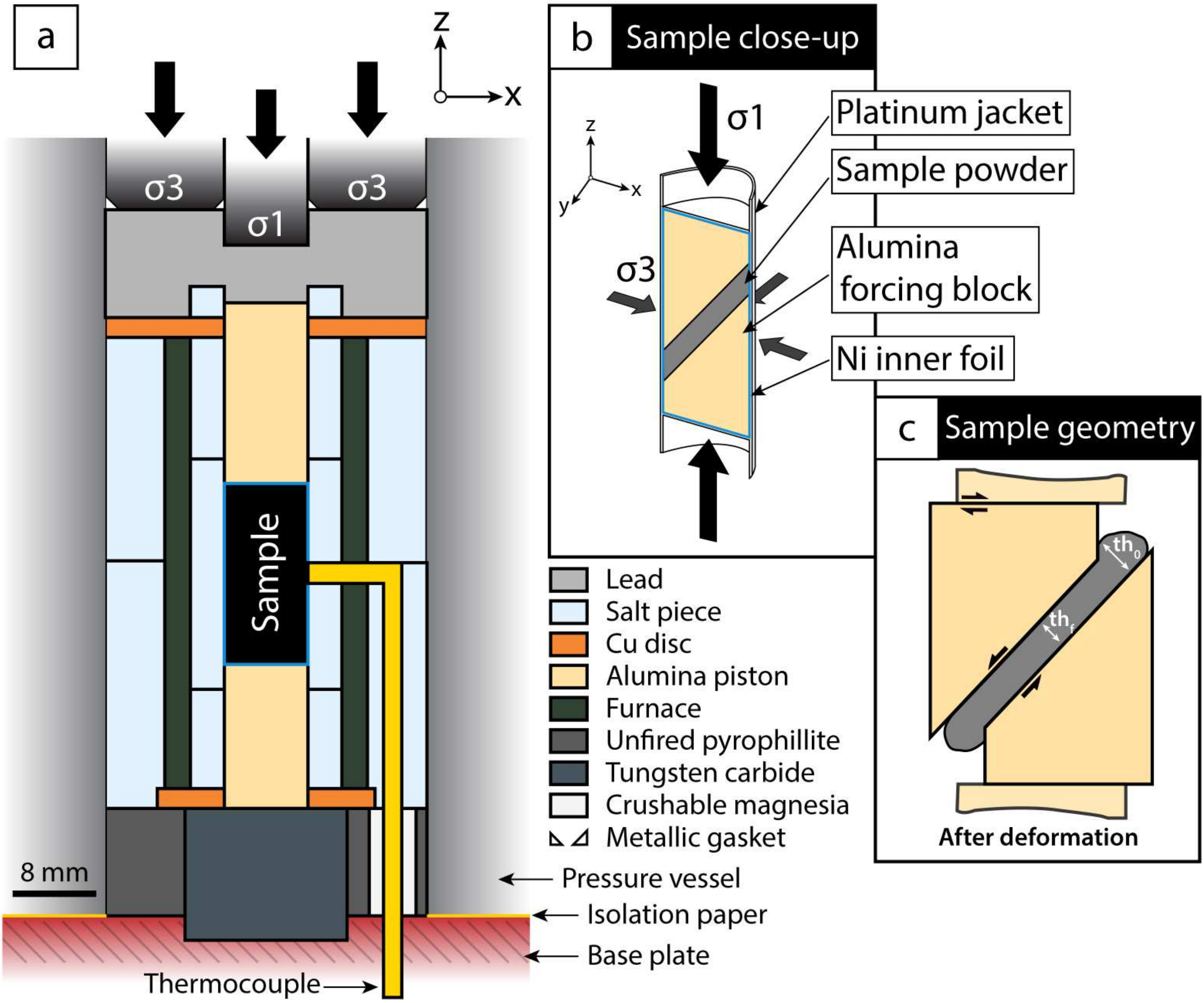
a
z
x
σ3
σ1
σ3
σ1
Sample
8 mm
Thermocouple
b
Sample close-up
z
x
y
σ1
σ3
Platinum jacket
Sample powder
Alumina
forcing block
Ni inner foil
c
Sample geometry
th0
thf
After deformation
Lead
Salt piece
Cu disc
Alumina piston
Furnace
Unfired pyrophillite
Tungsten carbide
Crushable magnesia
Metallic gasket
Pressure vessel
Isolation paper
Base plate

Fig. 1.

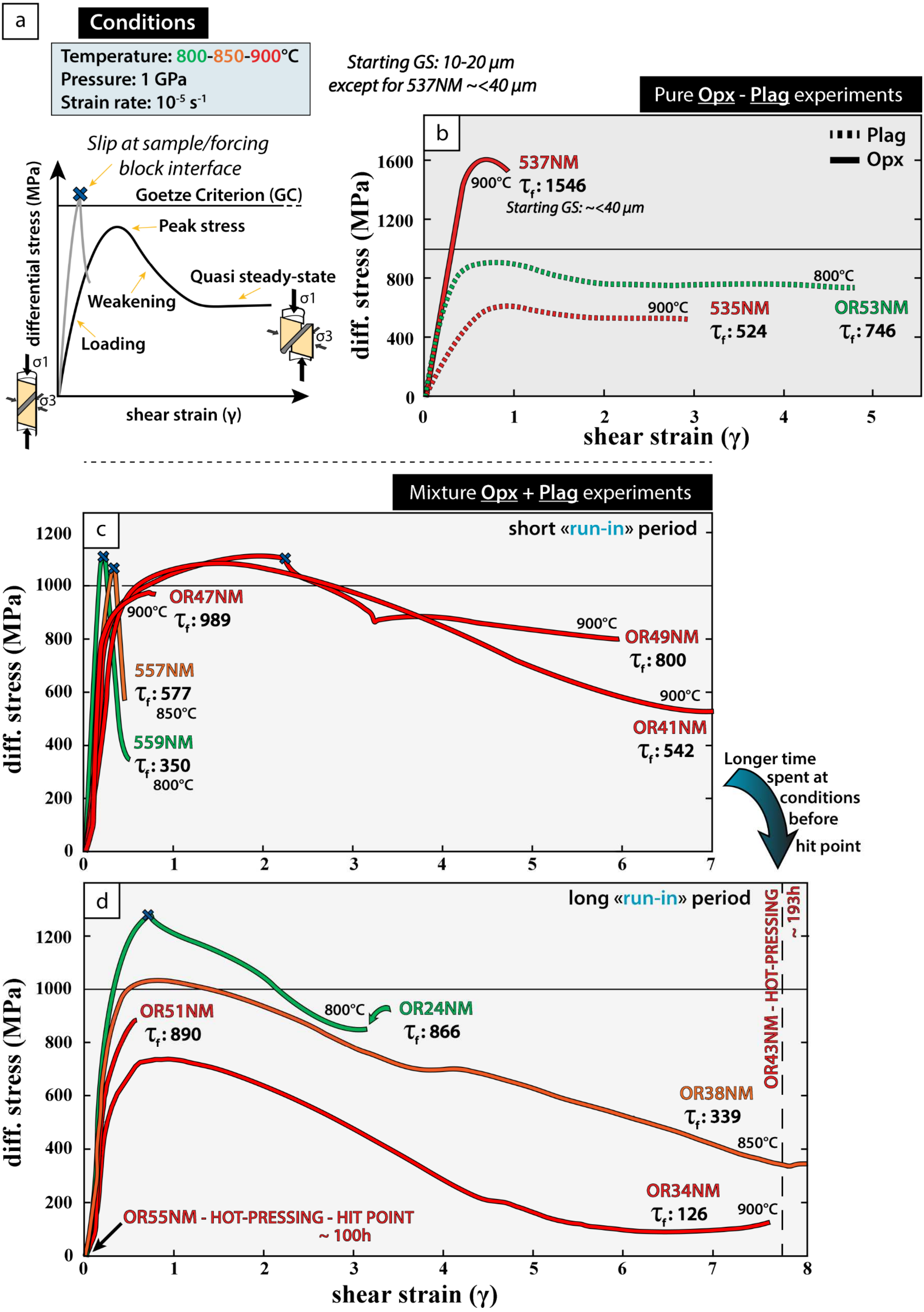
a
Conditions
Temperature: 800-850-900°C
Pressure: 1 GPa
Strain rate: 10-5 s-1
Starting GS: 10-20 µm
except for 537NM ~<40 µm
Slip at sample/forcing block interface
Goetze Criterion (GC)
Peak stress
Quasi steady-state
Weakening
Loading
differential stress (MPa)
shear strain (γ)
σ1
σ3
Pure Opx - Plag experiments
b
Plag
Opx
537NM
900°C
τf: 1546
Starting GS: ~<40 µm
800°C
900°C
535NM
τf: 524
OR53NM
τf: 746
diff. stress (MPa)
shear strain (γ)
Mixture Opx + Plag experiments
c
short «run-in» period
OR47NM
900°C
τf: 989
900°C
OR49NM
τf: 800
557NM
τf: 577
850°C
559NM
τf: 350
800°C
900°C
OR41NM
τf: 542
diff. stress (MPa)
Longer time spent at conditions before hit point
d
long «run-in» period
OR51NM
τf: 890
800°C
OR24NM
τf: 866
OR43NM - HOT-PRESSING ~ 193h
OR38NM
τf: 339
850°C
OR34NM
τf: 126
900°C
OR55NM - HOT-PRESSING - HIT POINT ~ 100h
diff. stress (MPa)
shear strain (γ)

Fig. 2.

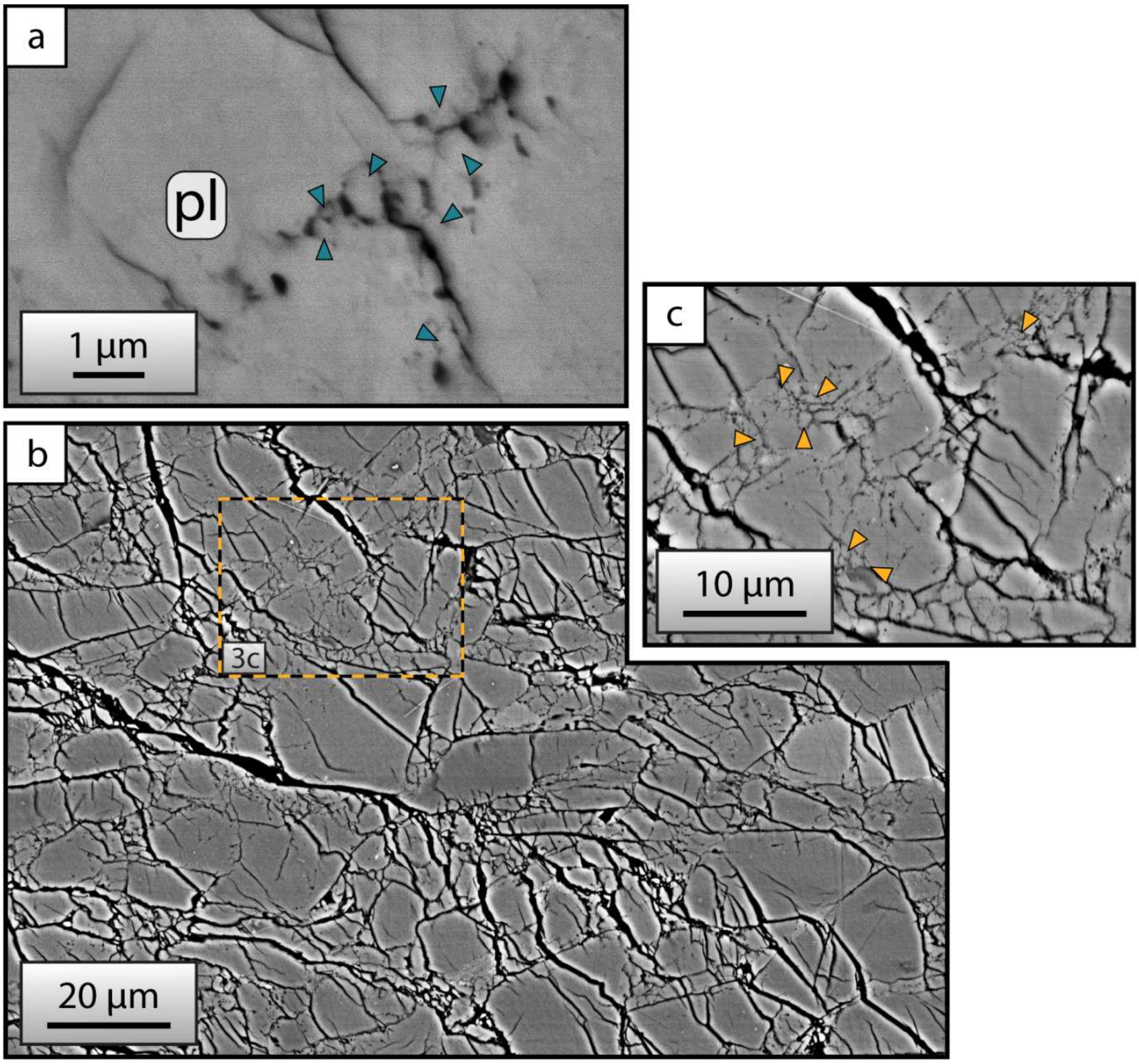

Fig. 3.

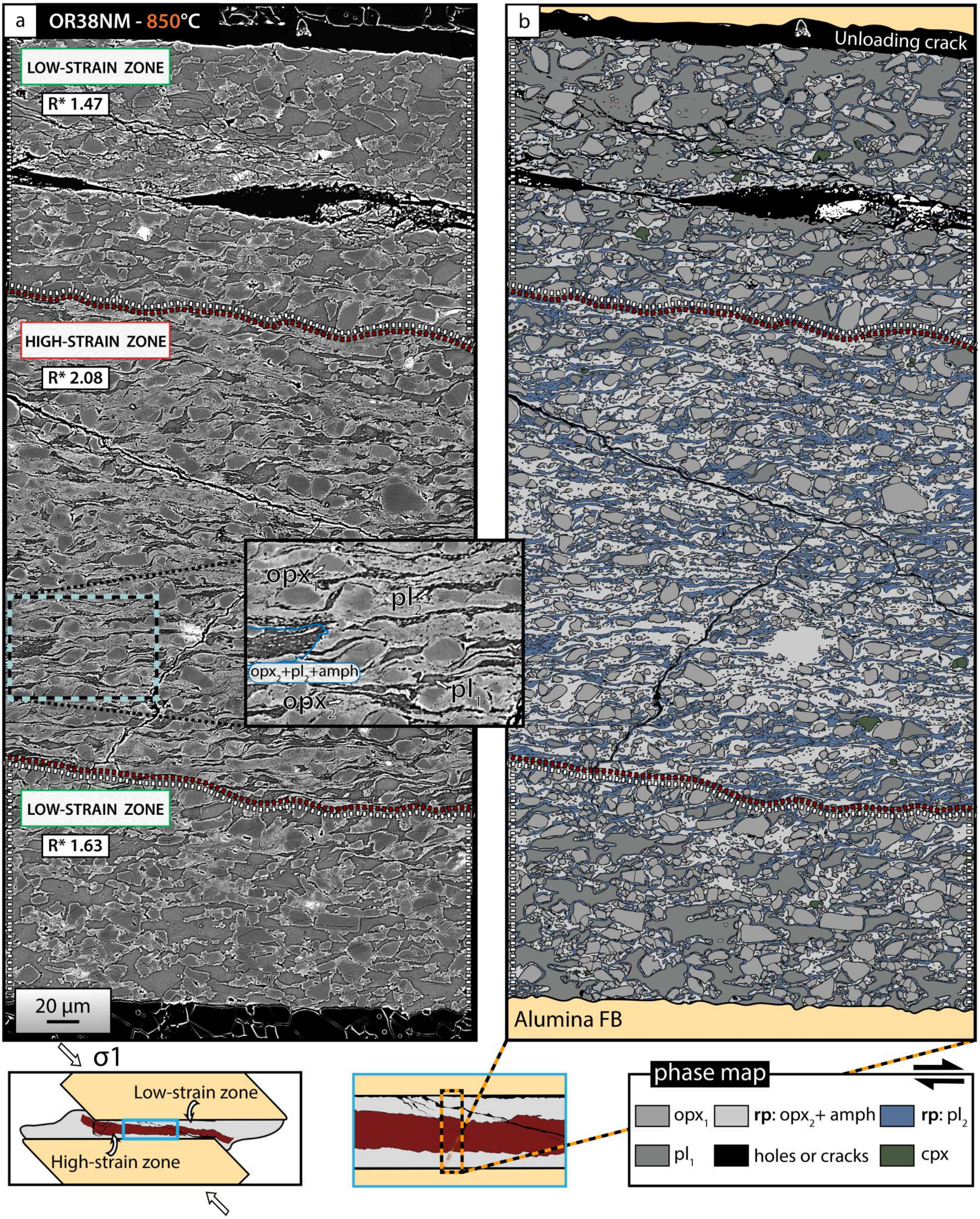
a
OR38NM - 850°C
LOW-STRAIN ZONE
R* 1.47
HIGH-STRAIN ZONE
R* 2.08
LOW-STRAIN ZONE
R* 1.63
20 µm
opx$_1$
pl$_2$
opx$_2$+pl$_2$+amph
opx$_2$
pl$_1$
b
Unloading crack
Alumina FB
σ1
Low-strain zone
High-strain zone
phase map
opx$_1$
rp: opx$_2$+ amph
rp: pl$_2$
pl$_1$
holes or cracks
cpx

Fig. 4.

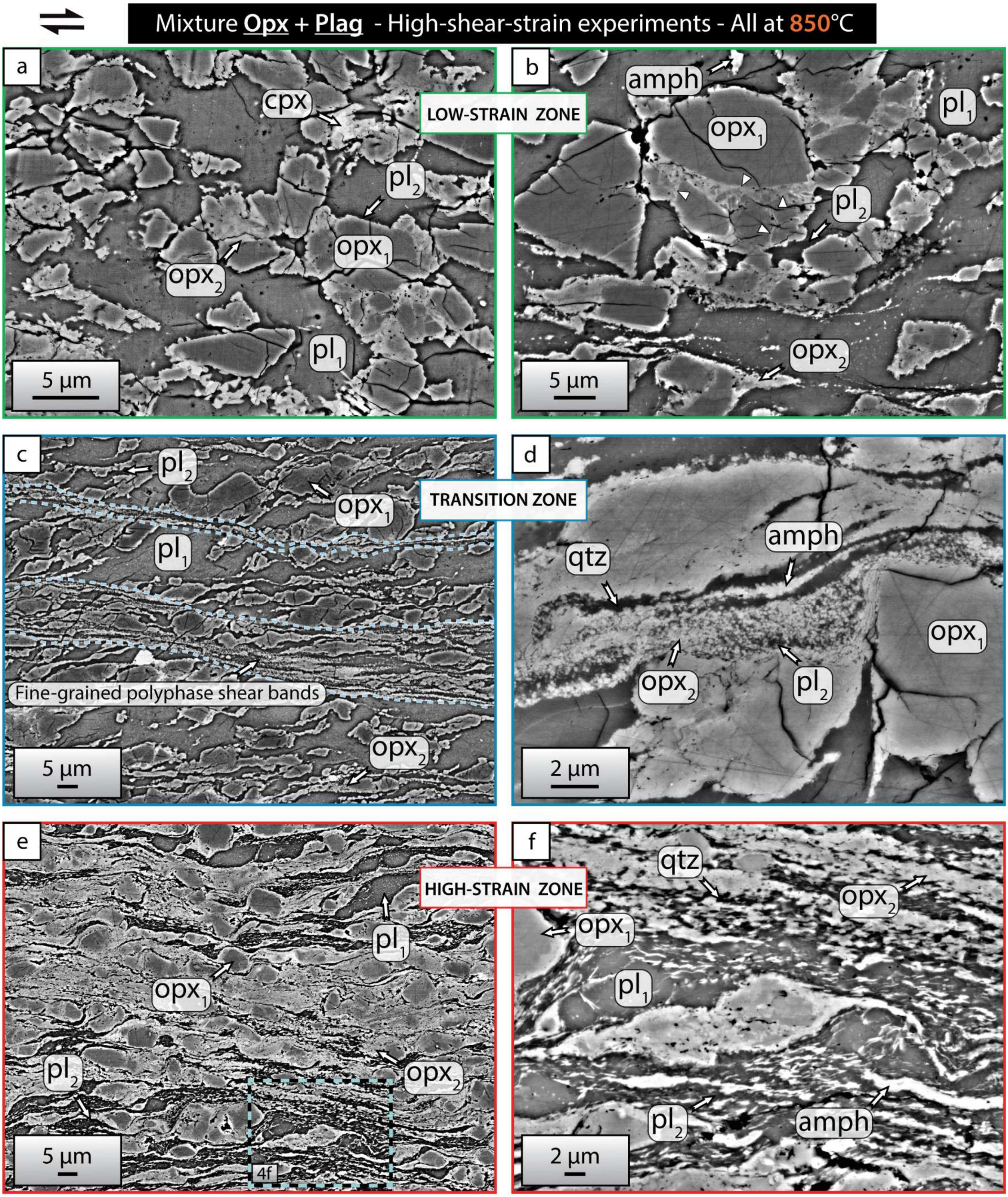
⇄
Mixture **Opx** + **Plag** - High-shear-strain experiments - All at 850°C
a
cpx
pl2
opx1
opx2
pl1
5 µm
b
amph
pl1
opx1
pl2
opx2
5 µm
LOW-STRAIN ZONE
c
pl2
opx1
pl1
Fine-grained polyphase shear bands
opx2
5 µm
d
amph
qtz
opx1
opx2
pl2
2 µm
TRANSITION ZONE
e
pl1
opx1
pl2
opx2
4f
5 µm
f
qtz
opx2
opx1
pl1
pl2
amph
2 µm
HIGH-STRAIN ZONE

Fig. 5.

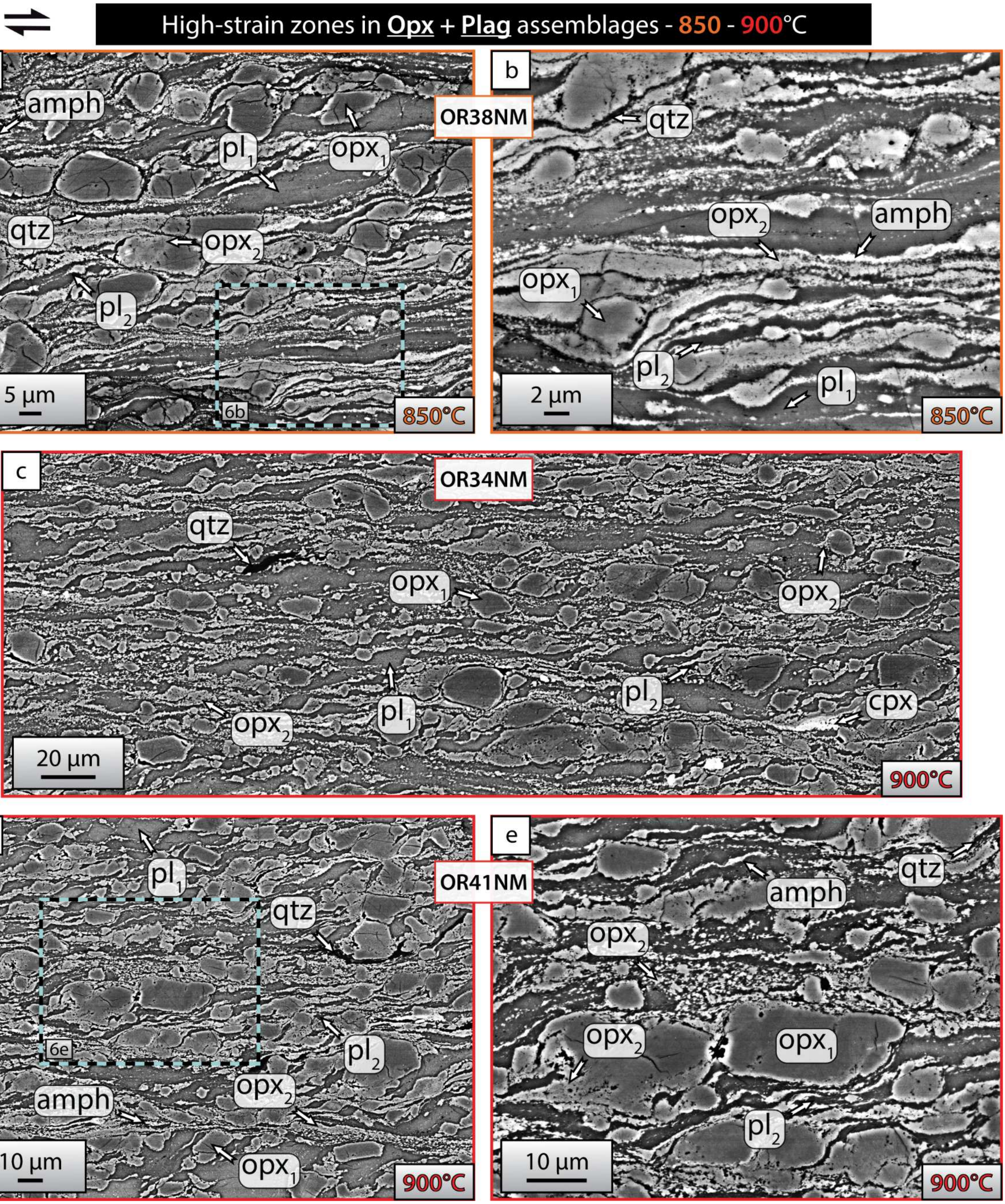
High-strain zones in Opx + Plag assemblages - 850 - 900°C
a
b
OR38NM
amph
pl1
opx1
qtz
opx2
pl2
6b
5 µm
850°C
qtz
opx2
amph
opx1
pl2
pl1
2 µm
850°C
c
OR34NM
qtz
opx1
opx2
pl1
pl2
cpx
opx2
20 µm
900°C
d
e
OR41NM
pl1
qtz
pl2
6e
amph
opx2
opx1
10 µm
900°C
amph
qtz
opx2
opx2
opx1
pl2
10 µm
900°C

Fig. 6.

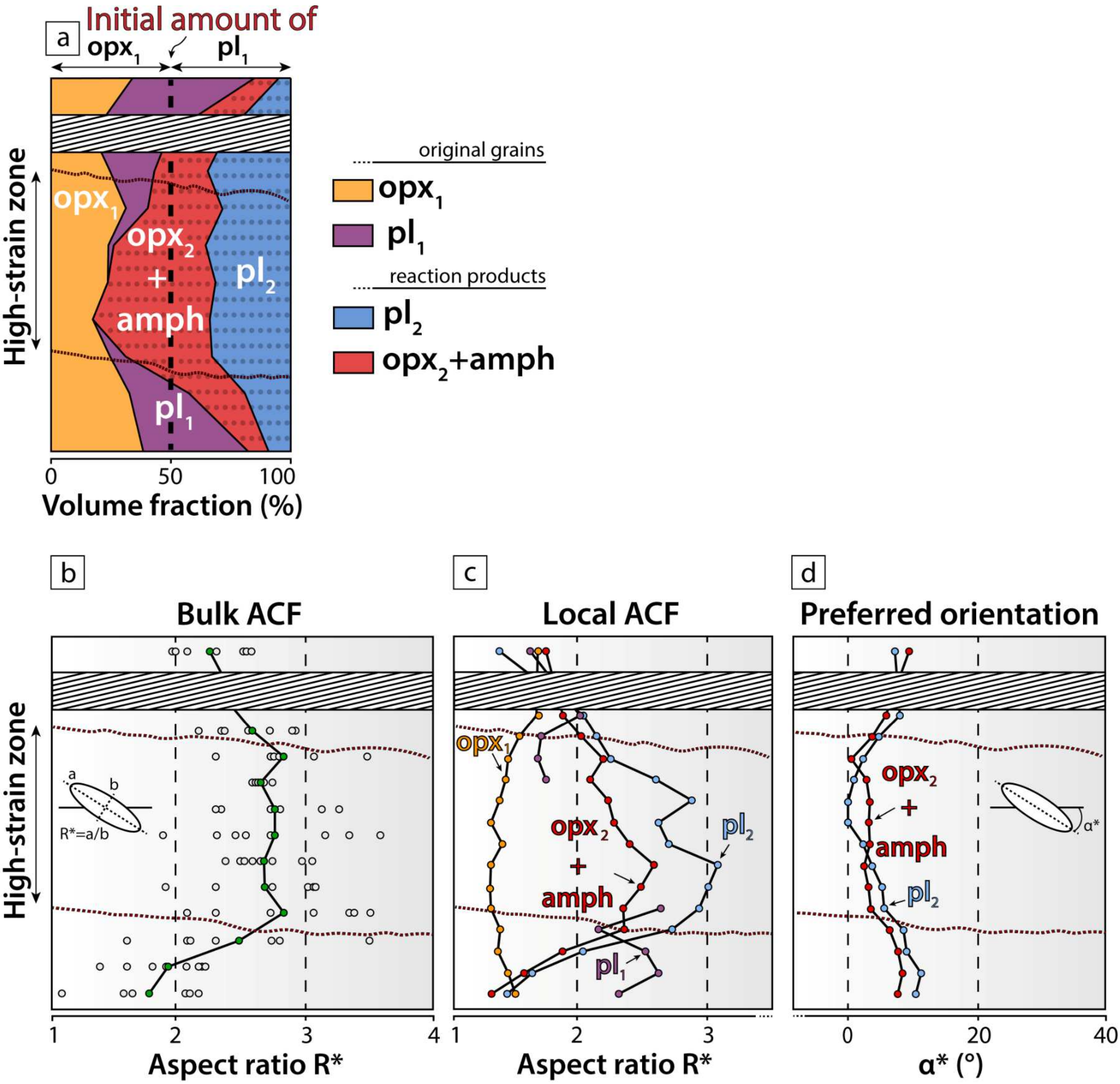
a
Initial amount of
opx1
pl1
High-strain zone
opx1
opx2
+
amph
pl2
pl1
0
50
100
Volume fraction (%)
original grains
opx1
pl1
reaction products
pl2
opx2+amph
b
Bulk ACF
High-strain zone
a
b
R*=a/b
1
2
3
4
Aspect ratio R*
c
Local ACF
opx1
opx2
+
amph
pl2
pl1
1
2
3
Aspect ratio R*
d
Preferred orientation
opx2
+
amph
pl2
α*
0
20
40
α* (°)

Fig. 7.

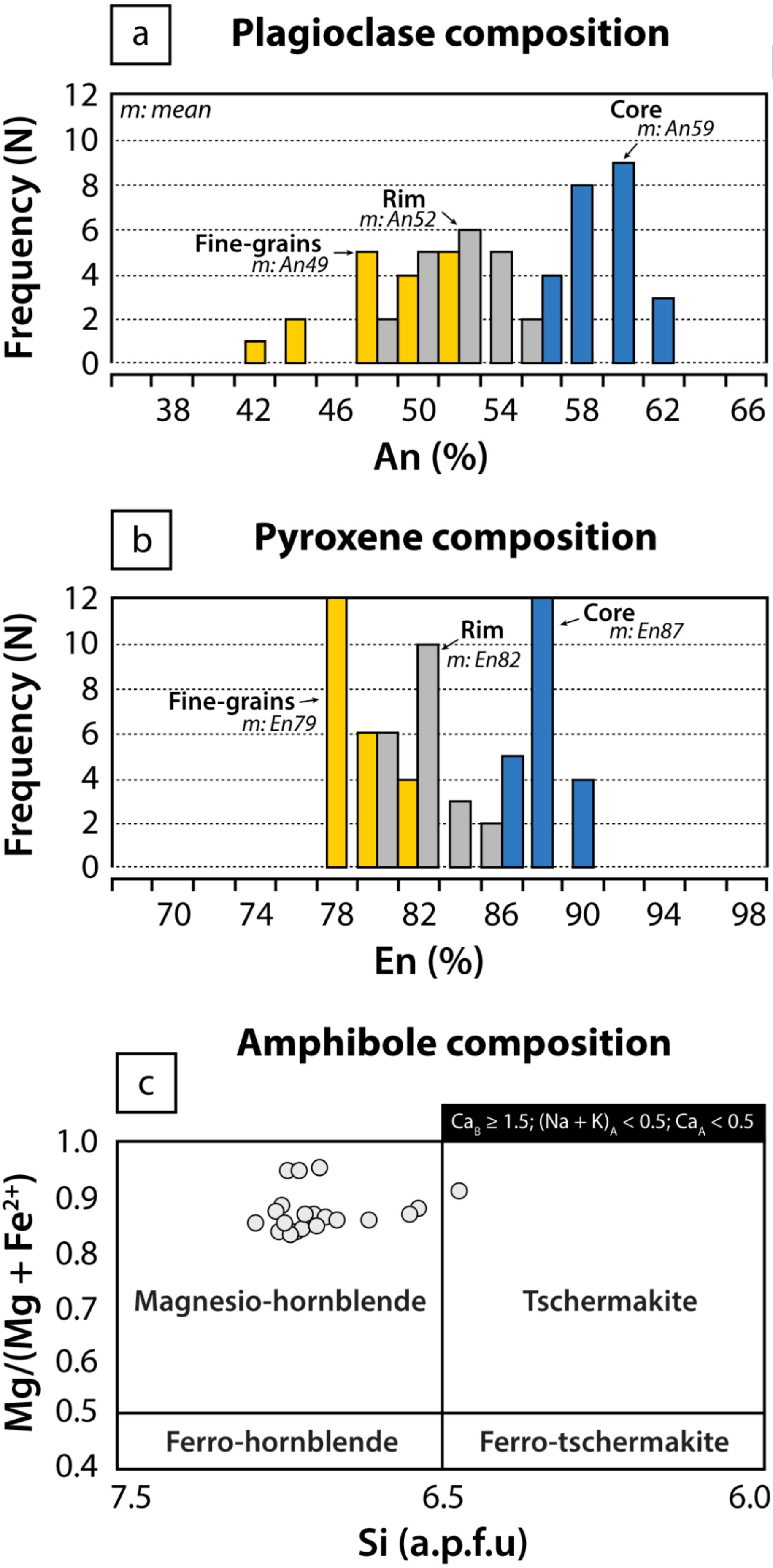
a
Plagioclase composition
m: mean
Core
m: An59
Rim
m: An52
Fine-grains
m: An49
Frequency (N)
0
2
4
6
8
10
12
38
42
46
50
54
58
62
66
An (%)
b
Pyroxene composition
Core
m: En87
Rim
m: En82
Fine-grains
m: En79
Frequency (N)
0
2
4
6
8
10
12
70
74
78
82
86
90
94
98
En (%)
c
Amphibole composition
Ca$_B$ ≥ 1.5; (Na + K)$_A$ < 0.5; Ca$_A$ < 0.5
Magnesio-hornblende
Tschermakite
Ferro-hornblende
Ferro-tschermakite
Mg/(Mg + Fe^{2+})
1.0
0.9
0.8
0.7
0.6
0.5
0.4
7.5
6.5
6.0
Si (a.p.f.u)

Fig. 8.

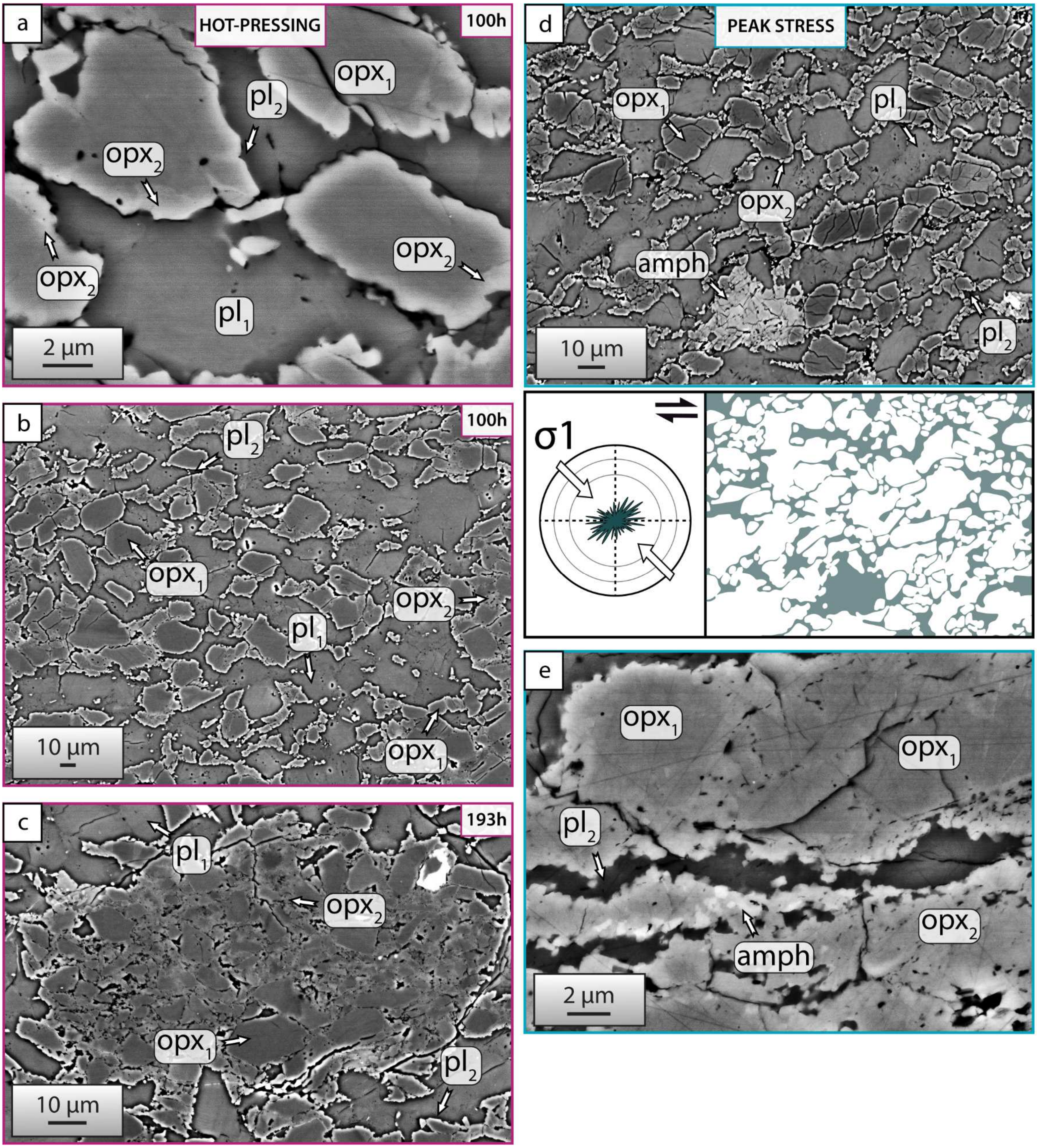
a
HOT-PRESSING
100h
opx$_1$
pl$_2$
opx$_2$
opx$_2$
opx$_2$
pl$_1$
2 µm
b
100h
pl$_2$
opx$_1$
opx$_2$
pl$_1$
opx$_1$
10 µm
c
193h
pl$_1$
opx$_2$
opx$_1$
pl$_2$
10 µm
d
PEAK STRESS
opx$_1$
pl$_1$
opx$_2$
amph
pl$_2$
10 µm
σ1
e
opx$_1$
opx$_1$
pl$_2$
amph
opx$_2$
2 µm

Fig. 9.

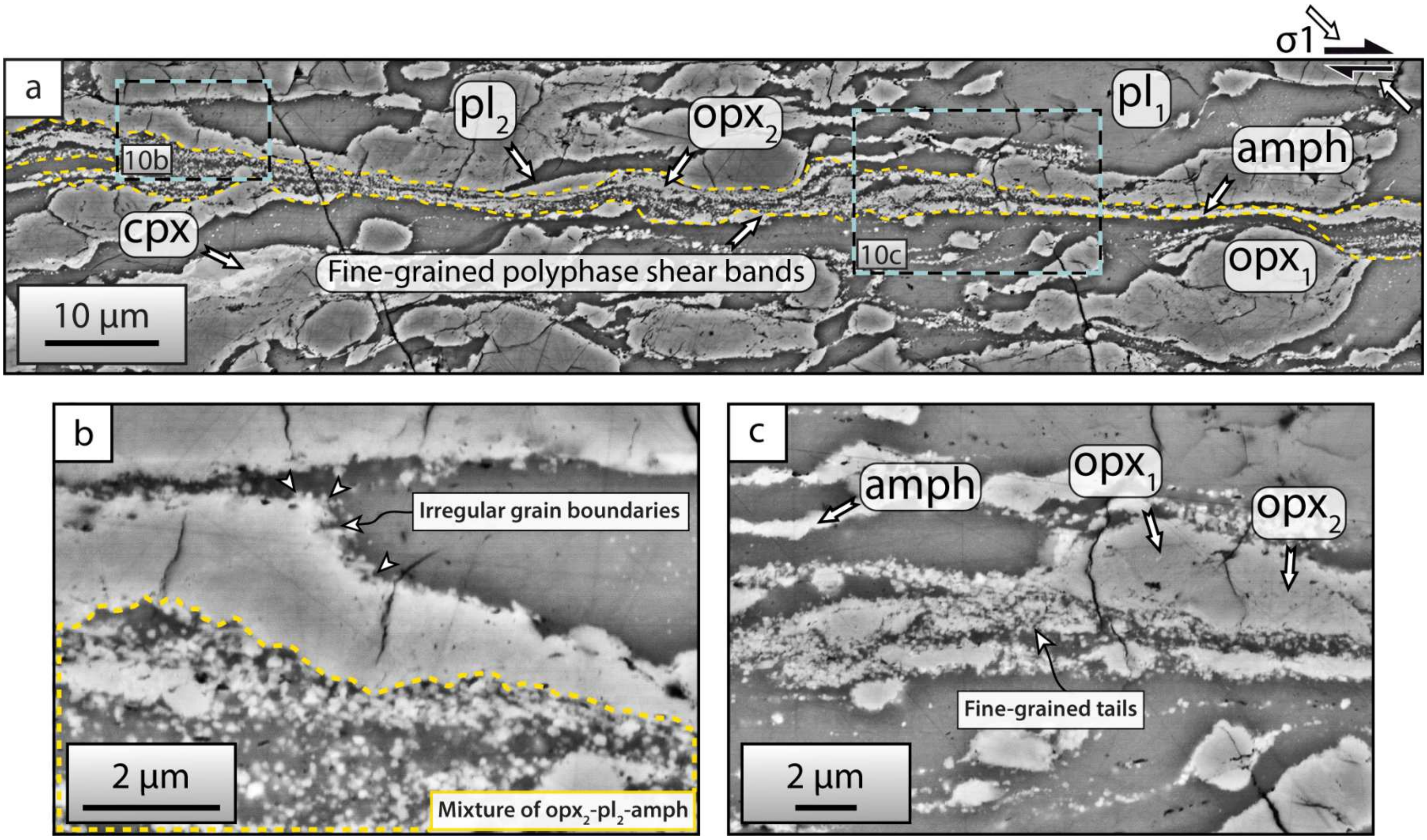
σ1
a
10b
10c
pl₂
opx₂
pl₁
amph
cpx
opx₁
Fine-grained polyphase shear bands
10 μm
b
Irregular grain boundaries
2 μm
Mixture of opx₂-pl₂-amph
c
amph
opx₁
opx₂
Fine-grained tails
2 μm

Fig. 10.

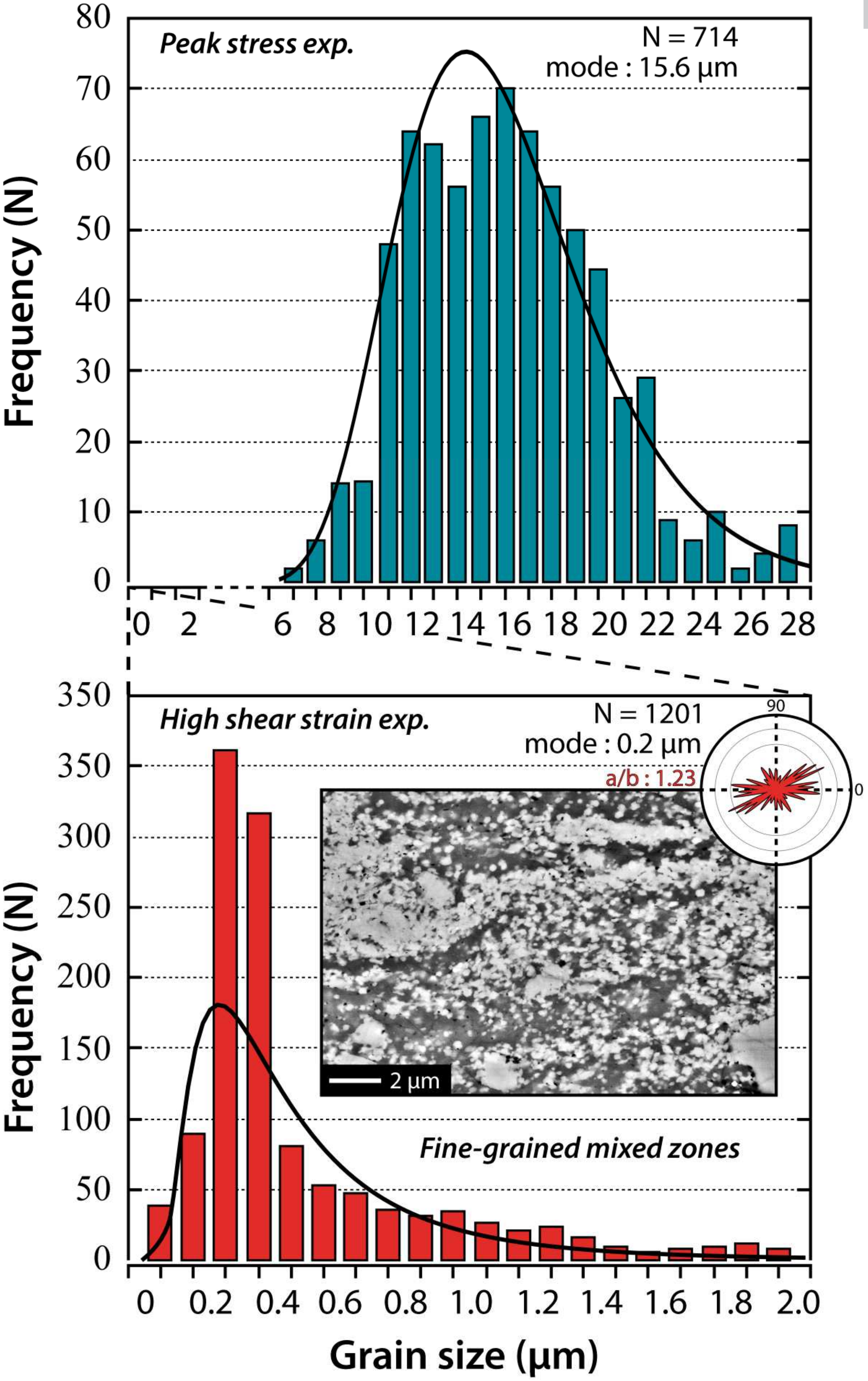
Peak stress exp.
N = 714
mode : 15.6 µm
Frequency (N)
0
10
20
30
40
50
60
70
80
0
2
6
8
10
12
14
16
18
20
22
24
26
28
High shear strain exp.
N = 1201
mode : 0.2 µm
a/b : 1.23
90
0
2 µm
Fine-grained mixed zones
Frequency (N)
0
50
100
150
200
250
300
350
350
0
0.2
0.4
0.6
0.8
1.0
1.2
1.4
1.6
1.8
2.0
Grain size (µm)

Fig. 11.

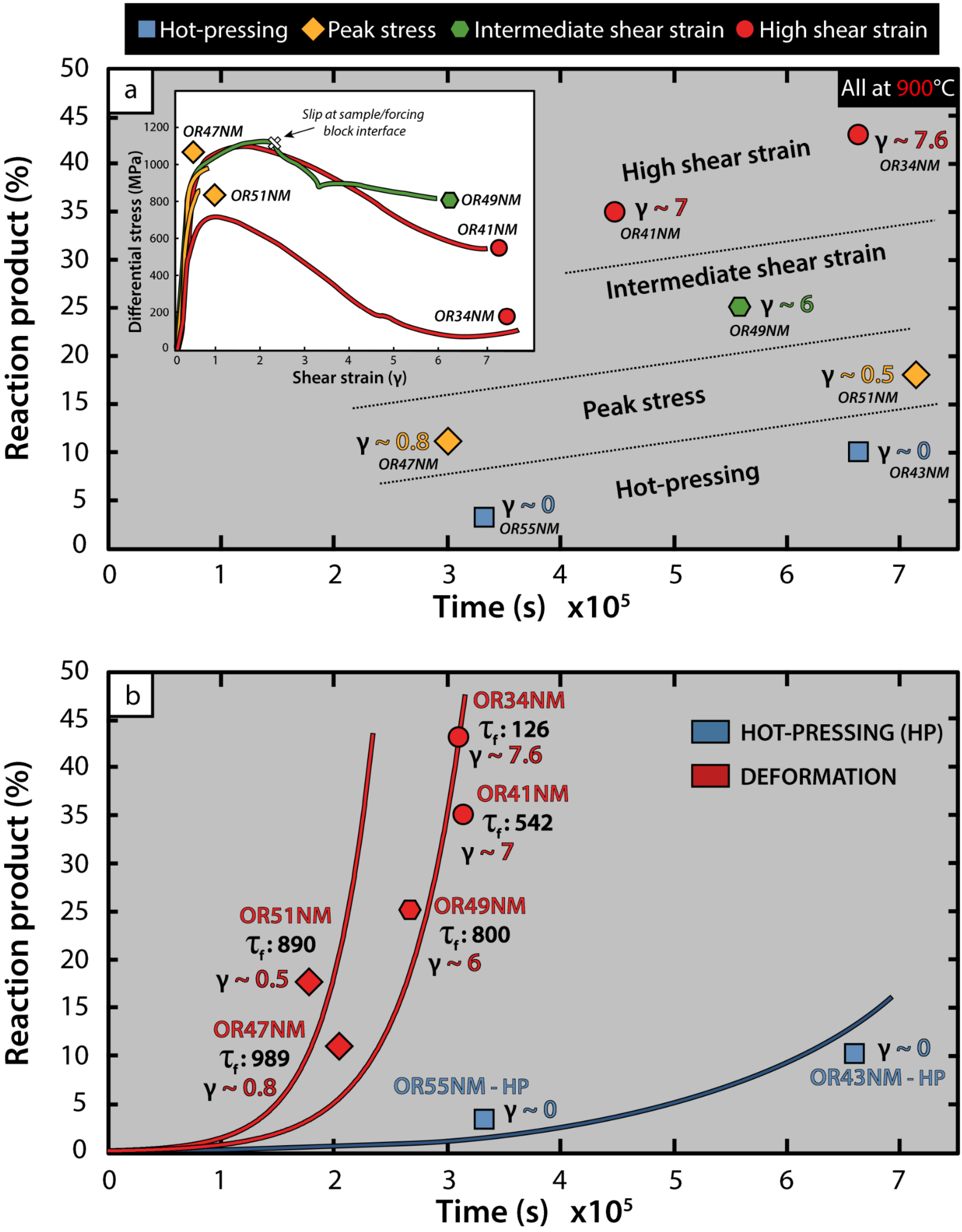

Hot-pressing
Peak stress
Intermediate shear strain
High shear strain
a
All at 900°C
Reaction product (%)
Time (s) x10⁵
High shear strain
Intermediate shear strain
Peak stress
Hot-pressing
γ ~ 7.6
OR34NM
γ ~ 7
OR41NM
γ ~ 6
OR49NM
γ ~ 0.5
OR51NM
γ ~ 0.8
OR47NM
γ ~ 0
OR43NM
γ ~ 0
OR55NM
Differential stress (MPa)
Shear strain (γ)
Slip at sample/forcing block interface
OR47NM
OR51NM
OR49NM
OR41NM
OR34NM
b
Reaction product (%)
Time (s) x10⁵
HOT-PRESSING (HP)
DEFORMATION
OR34NM
τf: 126
γ ~ 7.6
OR41NM
τf: 542
γ ~ 7
OR49NM
τf: 800
γ ~ 6
OR51NM
τf: 890
γ ~ 0.5
OR47NM
τf: 989
γ ~ 0.8
OR55NM - HP
γ ~ 0
OR43NM - HP
γ ~ 0

Fig. 12.

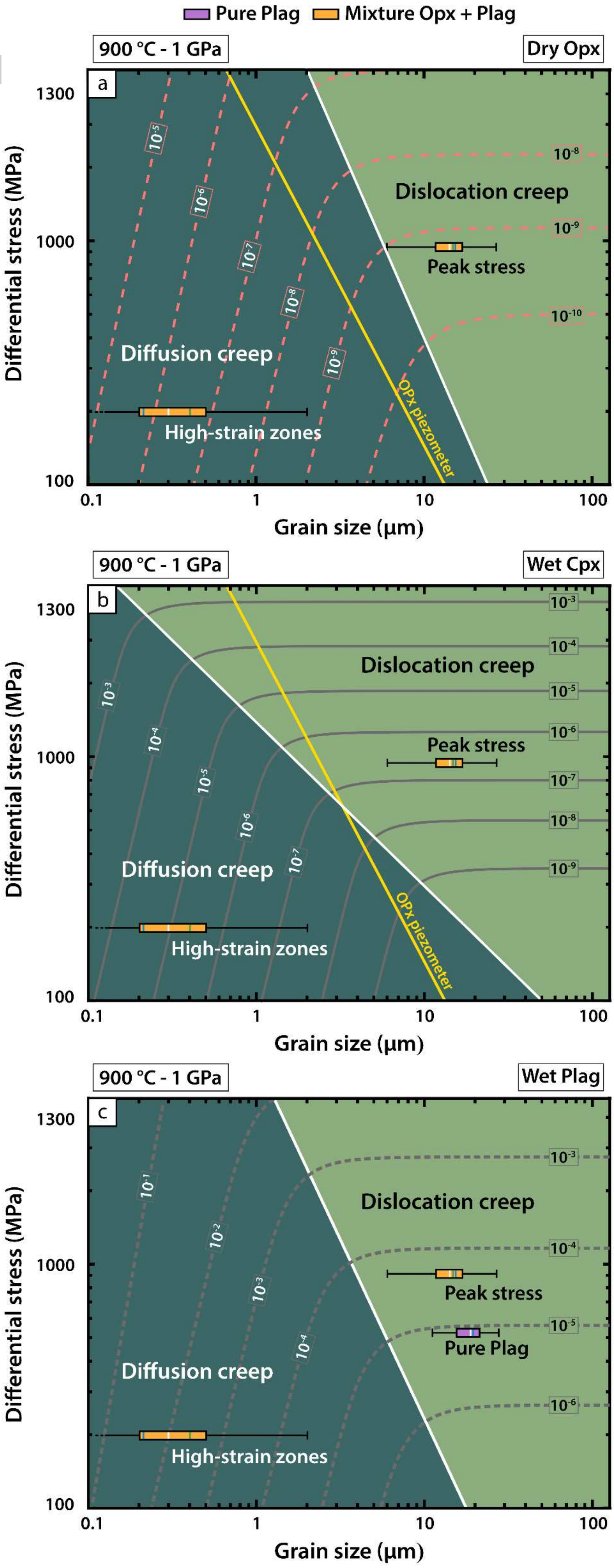
Pure Plag
Mixture Opx + Plag
900 °C - 1 GPa
Dry Opx
a
Dislocation creep
Diffusion creep
Peak stress
High-strain zones
OPx piezometer
10^{-5}
10^{-6}
10^{-7}
10^{-8}
10^{-9}
10^{-8}
10^{-9}
10^{-10}
1300
1000
100
0.1
1
10
100
Differential stress (MPa)
Grain size (μm)
900 °C - 1 GPa
Wet Cpx
b
Dislocation creep
Diffusion creep
Peak stress
High-strain zones
OPx piezometer
10^{-3}
10^{-4}
10^{-5}
10^{-6}
10^{-7}
10^{-3}
10^{-4}
10^{-5}
10^{-6}
10^{-7}
10^{-8}
10^{-9}
1300
1000
100
0.1
1
10
100
Differential stress (MPa)
Grain size (μm)
900 °C - 1 GPa
Wet Plag
c
Dislocation creep
Diffusion creep
Peak stress
Pure Plag
High-strain zones
10^{-1}
10^{-2}
10^{-3}
10^{-4}
10^{-3}
10^{-4}
10^{-5}
10^{-6}
1300
1000
100
0.1
1
10
100
Differential stress (MPa)
Grain size (μm)

Fig. 13.

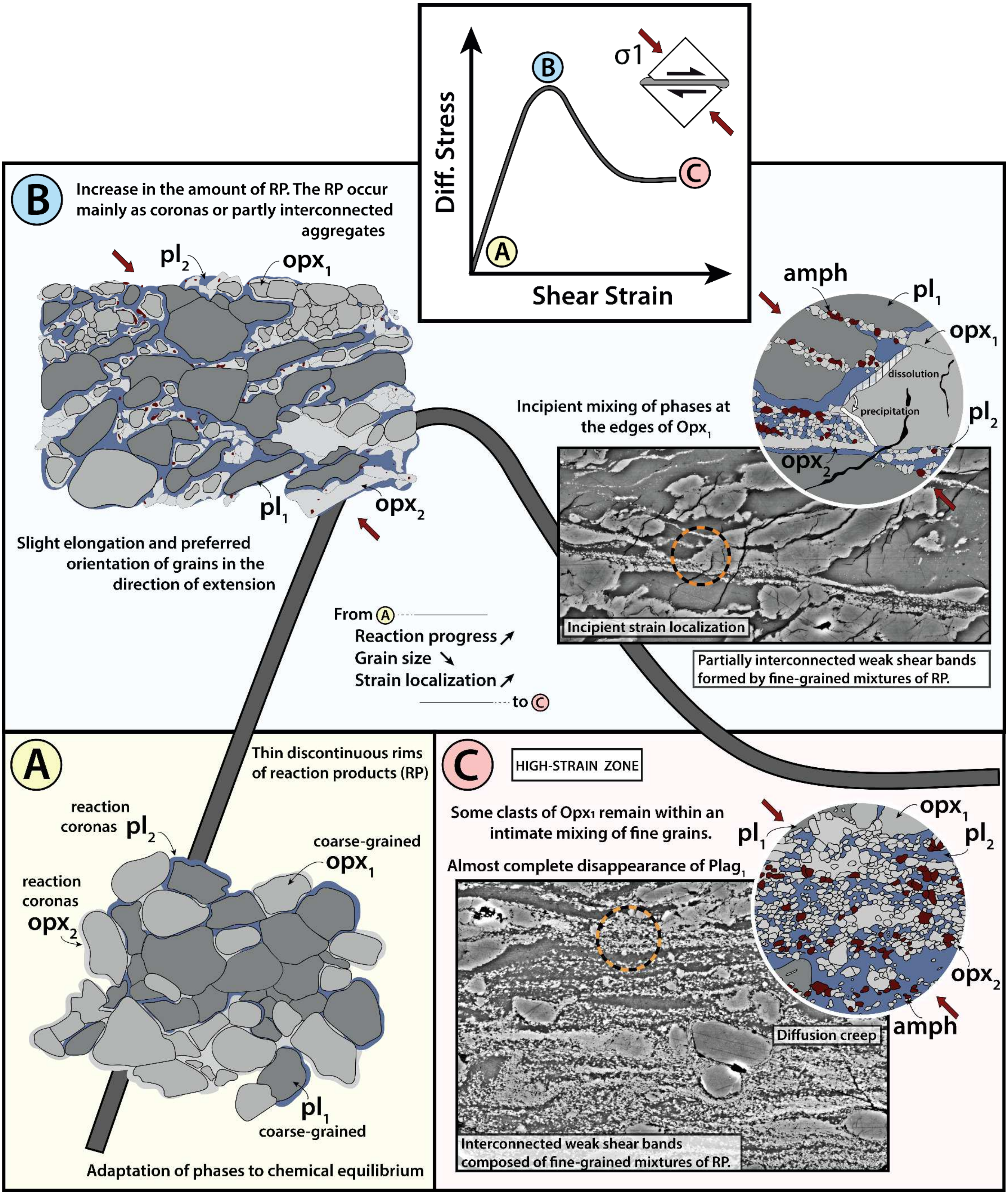
Diff. Stress
Shear Strain
A
B
C
σ1
B
Increase in the amount of RP. The RP occur mainly as coronas or partly interconnected aggregates
pl$_2$
opx$_1$
pl$_1$
opx$_2$
Slight elongation and preferred orientation of grains in the direction of extension
From A
Reaction progress ↗
Grain size ↘
Strain localization ↗
to C
amph
pl$_1$
opx$_1$
dissolution
precipitation
pl$_2$
opx$_2$
Incipient mixing of phases at the edges of Opx$_1$
Incipient strain localization
Partially interconnected weak shear bands formed by fine-grained mixtures of RP.
A
Thin discontinuous rims of reaction products (RP)
reaction coronas pl$_2$
coarse-grained opx$_1$
reaction coronas opx$_2$
pl$_1$ coarse-grained
Adaptation of phases to chemical equilibrium
C
HIGH-STRAIN ZONE
Some clasts of Opx$_1$ remain within an intimate mixing of fine grains.
Almost complete disappearance of Plag$_1$
pl$_1$
opx$_1$
pl$_2$
opx$_2$
amph
Diffusion creep
Interconnected weak shear bands composed of fine-grained mixtures of RP.

Fig. 14.

- Deformation considerably enhances the kinetics of mineral reactions.
- Diffusion creep is dominant in fine grained aggregates.
- Strain localization is due to the interplay between deformation and reaction.
- The degree of connectivity of the reacted material controls the bulk rheology.

Declaration of interests

☒ The authors declare that they have no known competing financial interests or personal relationships that could have appeared to influence the work reported in this paper.

☐The authors declare the following financial interests/personal relationships which may be considered as potential competing interests: